Current Nanoscience, 2021, *17*, 241-256

REVIEW ARTICLE

Pitting Corrosion of Biomedical Titanium and Titanium Alloys: A Brief Review

Yu-Wei Cui[1], Liang-Yu Chen[2,*] and Xin-Xin Liu[3]

[1]*School of Science, Jiangsu University of Science and Technology, Zhenjiang, Jiangsu, China;* [2]*School of Materials Science and Engineering, Jiangsu University of Science and Technology, Zhenjiang, Jiangsu, China;* [3]*School of Science, Jiangsu University of Science and Technology, Zhenjiang, Jiangsu, China*

ARTICLE HISTORY

Received: February 27, 2020
Revised: September 26, 2020
Accepted: October 20, 2020

DOI:
10.2174/1573413716999201125221211

Abstract: Thanks to their excellent corrosion resistance, superior mechanical properties and good biocompatibility, titanium (Ti) and Ti alloys are extensively applied in biomedical fields. Pitting corrosion is a critical consideration for the reliability of Ti and Ti alloys used in the human body. Therefore, this article focuses on the pitting corrosion of Ti and Ti alloys, which introduces the growth stages of pitting corrosion and its main influencing factors. Three stages, *i.e.* (1) breakdown of passive film, (2) metastable pitting, and (3) propagation of pitting, are roughly divided to introduce the pitting corrosion. As reviewed, corrosive environment, applied potential, temperature and alloy compositions are the main factors affecting the pitting corrosion of Ti and Ti alloys. Moreover, the pitting corrosion of different types Ti alloys are also reviewed to correlate the types of Ti alloys and the main factors of pitting corrosion. Roughly speaking, β-type Ti alloys have the best pitting corrosion resistance among the three types of Ti alloys.

Keywords: Pitting corrosion, titanium alloys, passive film, metastable pitting, pitting nucleation, β-type Ti alloys.

1. INTRODUCTION

Generally, biomedical materials are artificial or natural materials that are used to diagnose, treatment, repair or replace the dysfunctional tissues or organs and/or to enhance their functions in natural body [1-6]. In general, biomedical materials are differentiate into biomedical metallic materials, bioglass, bioceramics, bio-derived materials and biomedical polymer materials according to their compositions and properties [7-13]. Among these biomedical materials, biomedical metallic materials have good processability, high strength, good toughness, good anti-fatigue properties and other irreplaceable excellent properties as compared to other biomedical materials [14-17]. Therefore, biomedical metallic materials are mainly employed as load-bearing implant materials for a long-time use [18-23]. For example, biomedical metallic materials are frequently used for some total hip replacements as well as joint replacement surgeries, including knees, shoulders and elbows [24-28]. Other applications of biomedical metallic materials in the human body are intravascular stents, cardiac simulator, trauma and spinal fixation devices, heart valves and dentistry [24, 29-31]. Until recently, biomedical metallic materials demonstrate wider applications due to the flourish of additive manufacturing technology and other new technologies [29, 32-37].

To be functional as metallic implants in the human body, biomedical materials should meet the following requirements: high biocompatibility, adequate mechanical properties and good corrosion resistance in the human body [1]. Biocompatibility refers to the success of the interaction between biomaterials and biological cells in a biomedical environment [38]. High biocompatibility requires no adverse reactions, such as inflammation, infection, rejection and toxic action after implantation. Some elements such as Ti, Nb, Zr, Mo, Ta, W and Sn possess high biocompatibility, while some elements such as Al, V, Cr and so on are harmful to human body [29, 39-41]. Therefore, selecting appropriate alloying elements is of vital importance to design biomedical metallic materials. The demands of mechanical properties (including tensile characteristic, compressive characteristic and fatigue [42, 43]) of metallic materials vary with different purposes. For example, hip joint mainly requires high fatigue strength [44]. Elastic modulus, which is a fundamental mechanical property for bone replacement [45], has received special attention among the mechanical properties. If the elastic modulus of an implant is significantly greater than that of the replaced bone, stress shielding effect would produce between the implant and the natural bones [46-48]. The implant material with higher elastic modulus would bear more load when two materials with different elastic moduli are stressed together [46]. Actually, this phenomenon would result in bone atrophy and bone death [49]. Therefore, appropriate mechanical properties are another important factors for the success of implantation. Moreover, biomedical metallic implants would be corroded when immersed in the human

*Address correspondence to this author at the School of Materials Science and Engineering, Jiangsu University of Science and Technology, P.O. Box: 212003, Zhenjiang, China; Tel/Fax: 15805299631;
E-mail: lychen@just.edu.cn

physiological environment. Good corrosion resistance of metallic implants can avoid the damage of material properties (the degradation of metallic implants) [50]. Furthermore, there may be the impairment of host tissue due to the corrosion products from the implant [50]. Hence, good corrosion resistance is also necessary.

Based on the above considerations, the designed biomedical metallic materials are expected to have good biocompatibility, high strength, comparative elastic modulus with human bones and excellent corrosion resistance. As such, stainless steels were developed and successfully used as implant materials at the beginning of the 20th century [51]. Afterwards, Co–Cr-based alloys, Ti and Ti alloys were gradually available [52]. In the view of biocompatibility, stainless steels and Co–Cr-based alloys would release toxic ions (such as Cr, Ni and Co) in the human body, while Ti and Ti alloys are completely bioinert [47]. Meanwhile, from the aspect of mechanical properties, the stainless steels and Co–Cr-based alloys have significantly higher elastic moduli than the bones in the human body, as shown in Fig. (**1**) [47]. In comparison, Ti and Ti alloys have close elastic moduli to human bone, while they also possess enough strength [47, 53, 54]. Moreover, Ti and Ti alloys have the best corrosion resistance among these three types of materials, which can avoid the ion release and maintain the mechanical properties to the maximum extent in long-term implantation [49]. Therefore, Ti and Ti alloys receive considerable attentions in the biomedical field during recent decades.

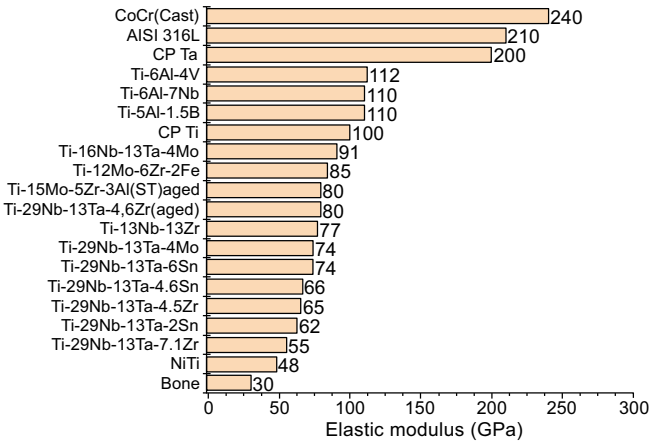

Fig. (1). Elastic moduli of various biomedical alloys and bone. (Reproduced with permission from ref. [47]. Copyright (2019), Wiley). (*A higher resolution / colour version of this figure is available in the electronic copy of the article*).

For a better understanding, a brief introduction with respect to the physical metallurgy of Ti and Ti alloys is offered as a background. Ti has a hexagonal close-packed (HCP) structure when the temperature below 882 °C and has a body-centered cubic (BCC) structure when the temperature is over 882 °C. Over 1668 °C, metallic Ti is melted. Commonly, Ti with HCP or BCC crystalline structures are called α–Ti or β–Ti, respectively. β–Ti is a high-temperature phase. However, appropriate additions of β–stabilizers (such as Zr, Nb and Ta) can maintain β–Ti at room temperature [55-58]. Similar to other hexagonal metallic materials, Ti alloys can be roughly categorized into α-type Ti alloys, (α+β)-type Ti alloys, and β-type Ti alloys according to their chemical compositions and phase constituents [59-64]. Different Ti alloys show different properties. Table **1** compares the mechanical properties of different types of Ti and Ti alloys [47, 65]. As seen from Table **1**, Ti alloys generally exhibit yield strength in the range of 544 and 1060 MPa. Meanwhile, the elastic moduli of β-type Ti alloys are between 55 and 85 GPa (Table **1**), close to that of human bone (Fig. **1**). Such mechanical properties enable Ti and Ti alloys to be satisfactory biomedical implants.

All types of Ti alloys possess excellent corrosion resistance in various environments because of the protective passive film formed on their surfaces in corrosive environments [66]. Especially, human body is an aqueous environment, which contains various salts and compounds. Hence, corrosion of Ti and Ti alloys is inevitable in the human body. The corrosion behavior of Ti and Ti alloys is strongly depend on the conditions of environment. Some aggressive ions, such as Cl^-, Br^-, F^-, I^-, *etc*., would lead to the pitting corrosion of Ti and Ti alloys [67]. Pitting corrosion is the accelerated dissolution of metals in a small region, which results from the local breakdown of protective passive film [68]. In human-body, once pitting corrosion of implants takes place, implants would rapidly age. As a result, pitting corrosion has great destructiveness and hidden trouble. To better understand the mechanism of pitting corrosion is an effective way to provide theoretical basis for the improvement in the pitting resistance of Ti and Ti alloys. Therefore, the investigation of pitting corrosion of titanium in the human environment is of great significance. This review introduces the applications of Ti and Ti alloys in the first place. During the service of Ti and Ti alloys, corrosion is inevitable in various corrosive environments, which promotes the formation of passive film on the surfaces of Ti and Ti alloys. Pitting, as a local phenomenon, always takes place on the passivated Ti and Ti alloys. Hence, pitting corrosion of Ti and Ti alloys is illustrated according to pitting nucleation and growth as well as their influencing factors. Due to their different chemical compositions, different types of Ti and Ti alloys exhibit distinct corrosion behavior and pitting behavior in a variety of corrosive environments. Therefore, the pitting corrosion of various Ti and Ti alloys is also reviewed [47, 65, 69-71].

2. PITTING CORROSION THEORY

2.1. Stages of Pitting

The formation of pitting corrosion needs a process. There is a long period of time from pit initiation to pit nucleation. Sometimes, this period maintains up to a few months or one year [68]. The surface scratches, inclusions, discontinuity and so on would become the preferential sites of pit initiation for metals. Once the pit is presented on the metal surface, it would continue to grow up in most cases. The process of pitting corrosion can be divided into three stages: (1) breakdown of passive film, (2) metastable pitting, and (3) propagation of pitting [72-75]. Fig. (**2**) exhibits primary processes

Table 1. Mechanical properties of various Ti and Ti alloys for biomedical applications.

Alloy	Phase Constituent	Tensile Strength (MPa)	Yield Strength (δy)	Elongation (%)	Elastic Moduli (GPa)
Pure Ti	α	240 – 550	170 – 485	15 – 24	102 – 104
Ti–6Al–4V (annealed)	α+β	895 – 930	825 – 869	6 – 10	110 – 114
Ti–6Al–7Nb	α+β	900 – 1050	880 – 950	8.1 – 15	114
Ti–5Al–2.5Fe	α+β	1020	895	15	112
Ti–5Al–1.5B	α+β	925 – 1080	820 – 930	15 – 17.0	110
Ti–15Sn–4Nb–2Ta–0.2Pd					
(annealed)	α+β	860	790	21	89
(aged)	α+β	1109	1020	10	103
Ti–15Zr–4Nb–4Ta–0.2Pd					
(annealed)	α+β	715	693	28	94
(aged)	α+β	919	806	18	99
Ti–13Nb–13Zr (aged)	β	973 – 1037	836 – 908	10–16	79–84
Ti–12Mo–6Zr–2Fe (annealed)	β	1060 – 1100	100 – 1060	18–22	74–85
Ti–15Mo (annealed)	β	874	544	21	78
Ti–15Mo–5Zr–3Al (aged)	β	1060 – 1100	1000 – 1060	18–22	
Ti–15Mo–2.8Nb–0.2Si (annealed)	β	979 – 999	945 – 987	16–18	83
Ti–35.3Nb–5.1Ta–7.1Zr	β	596.7	547.1	19.0	55.0
Ti–29Nb–13Ta–4.6Zr (aged)	β	911	864	13.2	80
Ti–24Nb–4Zr–8Sn	β	665 – 830	563 – 700	13 – 15	46 – 55
Ti-25Nb-3Zr-3Mo-2Sn	β	622 – 716	308 – 592	32 – 37	55 – 78

of pitting corrosion. In the following paragraphs, these three stages of pitting corrosion would be introduced in detail.

Breakdown of passive film.-The pitting process about the breakdown of passive film and pit initiation is rarely known [68]. Usually, passive film is considered as a simple inert layer which covers the metal substrate and prevents the ingression of corrosive ions from environments [68]. The stage of breakdown is very rapidly observed or examined. This stage also takes place in a small area (even in nano-scale) and therefore the nucleation currents are very small (although the current densities in this stage may be very large) [76]. A dynamic passive film should be considered during corrosion, which is critical to establish the relationship between the breakdown of passive film and the pit initiation [68]. Three models have been proposed in the last decade [77]: (1) the first model proposes that the local dissolution of metal initiates the pit without destroying passive film; (2) the second model assumes that the breakdown of passive film before pit initiation; (3) the third model postulates that the passive film would be thinned until the exposure of bare metal to corrosive environment. Accordingly, theories for the breakdown of passive film and pit initiation can be categorized into three mechanisms: penetration mechanism, film-breaking mechanism and adsorption mechanism [78]. However, these three mechanisms cannot be identified up to now.

The penetration mechanism was firstly proposed by Hoar *et al*. [79]. They found that the passive films of alloys would be penetrated by aggressive ions under relatively high potentials. Later, a better penetration mechanism was gradually established. Zhang *et al*. [80] discussed the mechanism of chloride-induced passivity breakdown in atomic scale. They postulated that the interfaces of nanocrystals and amorphous phases provide tunnels for Cl^- permeation. Cl^- eventually reaches the metal/passive film interface through these interconnected tunnels. Consequently, aggressive dissolution would be promoted by the accumulated Cl^- (the same as other aggressive ions). Fig. (**3**) illustrates the mechanism of the chloride-induced passivity breakdown in detail [80]. After the formation of passive film on metal substrate, Cl^- is adsorbed on the surface of passive film (Fig. **3a** and **3b**). Cl- can permeate along the tunnels provided by the interfaces of nanocrystals and amorphous phases, resulting in an undulated interface of passive film and substrate (Figs. **3c** and **3d**) [80]. On other hand, if the tunnels are not interconnected, Cl^- is unable to get through (Fig. **3d**) [80].

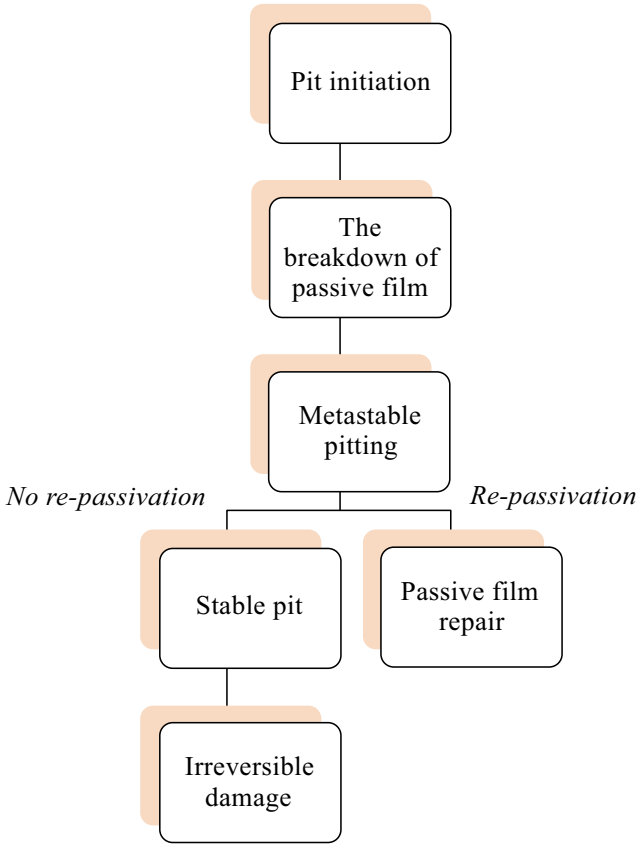

Fig. (2). Schematic illustration of the processes of pitting corrosion. (*A higher resolution / colour version of this figure is available in the electronic copy of the article*).

As known, the corrosion of metals is inhibited by the passive film formed on their surfaces. The breakdown of passive film leads to the ingression of aggressive ions, subsequently results in the formation of pits. Therefore, for film-breaking mechanism, passive film is in a breakdown-repair alternating state [81]. Hoar *et al.* [77] assumed that the passive film would suffer mechanical stress after being in contact with aggressive electrolyte and then the passive film is damaged by pores and flaws due to the change of interfacial force. Zhang *et al.* [80] deduced the local breakdown events due to surface tension effect; the proposed schematic diagram is shown in Fig. (**4**) [80]. A considerable number of Cl^- are inhomogeneously adsorbed on the surface of naked metal at the beginning of corrosion (Fig. **4a**) [80]. After permeation of Cl^-, high-concentration Cl^- leads to the quick dissolution of metal, which induces the inhomogeneous growth rate of passive film (Fig. **4b**) [80]. Undulated interface produces convex and concave, which would induce mechanical stress and cause local breakdown of passive film (Fig. **4c** and **4d**) [80]. Sato *et al.* [82] found that when the thickness of passive film reaches a certain thickness, breakdown taken place on account of electrostriction. Frankel [68] proposed that the electrostriction and surface tension effect in the weak sites would induce local breakdown events, which can be repaired in non-aggressive environments. However, re-passivation would be restrained in aggressive environments and the possibility of healing is lower [68].

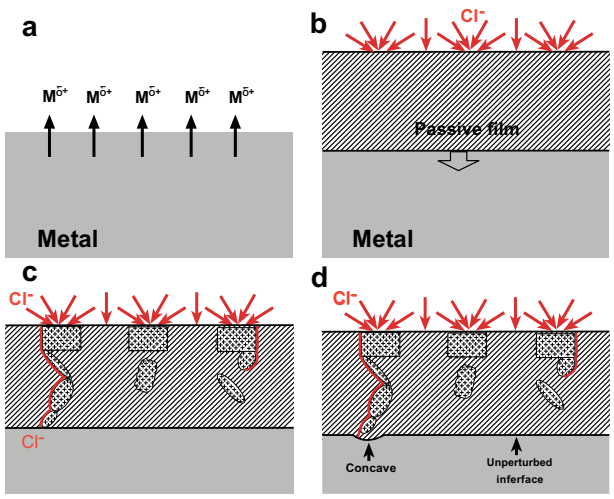

Fig. (3). Schematic diagram of the mechanism of chloride-induced passivity breakdown: (**a**) bare metal exposure to corrosive environment, (**b**) the formation of passive film and the adsorption of chloride ions, (**c**) the interfaces of nanocrystals and amorphous phase provides tunnels for Cl^- ions heterogeneously penetrating and (**d**) the formation of undulated interface of passive film and substrate. (Reproduced with permission [80]. Copyright (2018), Nature). (*A higher resolution / colour version of this figure is available in the electronic copy of the article*).

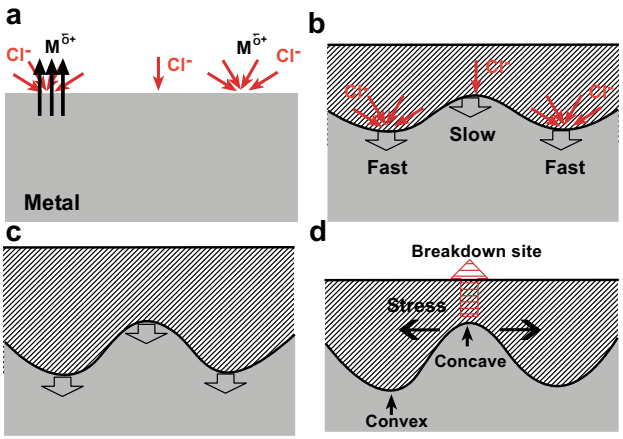

Fig. (4). Schematic diagram for the local breakdown of passive film: (**a**) the heterogeneous adsorption of Cl^- on the surface of naked metal in corrosive environment, (**b**) the inhomogeneous growth of passive film under the effect of Cl^-, (**c**) the deterioration of undulated interface and (**d**) the local breakdown induced by mechanical stress. (Reproduced with permission from ref. [80]. Copyright (2018), Nature). (*A higher resolution / colour version of this figure is available in the electronic copy of the article*).

Adsorption mechanism was the first proposed based on the conception of competitive adsorption of aggressive ions and oxygen ions [68]. Hoar *et al.* [83] found that the adsorption of aggressive ions at the surface of oxide film promotes the transfer of metal cations from oxide to electrolyte. This process results in the thinning of passive film, which may

be eventually removed [81]. As such, the local dissolution of passive film ensues [81]. Furthermore, there are at least several monolayers of passive film as compared to the adsorbed oxygen layer [68]. Under constant anode potential, some local adsorbed substances would lead to the local thinning of passive film. As a result, the strength of local electric field would significantly increase. Finanlly, a complete breakdown of passive film and pit initiation taken place [77, 81].

Metastable pitting.-Usually, metastable pits are considered as the growth of pits in the limited time before repassivation of local substrate [68]. Metastable pits are often micron-sized and their lifetimes are up to couple of seconds [68]. Many characterization methods are applied for better understanding about metastable pitting. For instance, statistical techniques are used to evaluate the intensity of pitting [84]. Besides, potentiostatic statistics is applied to analyze the current transients which are caused by metastable pitting [84]. According to a given applied potential, a few fluctuations of small current transients would be found before stable pitting takes place. Therefore, each nucleation event is accompanied by a sharp anodic current transient, which demonstrates quick re-passivation of local substrate [85]. These small current transients also indicate the formation, growth and annihilation of metastable pits [86]. Jiang *et al.* [67] studied the influence of Cl^- on Ti products, which is based on the constant potential statistics using the recorded current transients. They found that the amplitude and number of current transients increase with increasing the concentration of Cl^- [67]. Meanwhile, the random appearance of current transients manifests the stochastic properties of metastable pitting events. Actually, Jiang *et al.* [84] proposed an approach about the quantitative determination of metastable pitting based on the charge integration of current transients. They obtained a pit density (the number of metastable pits per unit area) of 1.0×103 cm^{-2} h^{-1} in 0.6 M NaCl solution at 0.5 VSCE, which has a typical radius of 0.12 μm [84]. As known, Ti and Ti alloys have been widely applied in the biomedical industry. Therefore, even a small quantity of metal ions releasing into human body may change the biological performance of Ti implants. Although stable pitting corrosion may be rare in the biomedical environment, metastable pitting corrosion, as the primary source of metal ion release, may play a vital role in the biological properties of implants [87]. Therefore, the investigation of metastable pitting is also of great significance for biomedical Ti and Ti alloys.

The development of metastable pitting is related either to the formation of stable pitting or to the appearance of repassivation. If the growth rate of metastable pitting is greater than re-passivation rate of local substrate, there would be a tendency of stable pitting, especially in solutions containing aggressive ions. Conversely, the passive film would be repaired. Although the material is passivated again, the local thickness of passive film is below the regions where no pitting corrosion takes place. Such a case would enhance the probability of the recurrence of pitting corrosion and the passive film may crack again under stress states [88, 89].

Propagation of pitting.-The growth of metastable pits is complex. There are many different models for the growth of metastable pits. For instance, Frankel [68] considered that the crucial factor for the growth of metastable pits is the metastable pits covered by passive film. The film is porous, which results in the diffusion of dissolved products in the pores and the aggressive ions from the environment. These micropores cause current convergence which brings about a higher impedance of the local region, while the growth of metastable pits is controlled by passive film impedance [68]. Therefore, the passive film with high impedance facilitates the growth of metastable pits. Otherwise, once the passive film ruptures, metastable pits would disappear because of repassivation. As such, the rate of the propagation of pits would be significantly fast once a pit is formed. The growth rate of pit depends on the electrolyte concentration inside, the potential at the pit bottom and material compositions [68]. Laycock *et al.* [90] proposed a model for the propagation of corrosion-pitting using a two-dimensional finite element method. They used the dissolution kinetics to simulate the growth of pits and found that the propagation of pitting requires a higher applied potential as compared to the pitting initiation.

There are numerous growth models regarding the propagation of pitting. At present, the existence of acidizing autocatalytic in pits is generally accepted [68, 91, 92]. Once a pit is formed, the metal in the pit is in an active state as anode and the other surface of metal is in a passive state as cathode. Therefore, a micro-galvanic corrosion cell is formed [93-95]. The anodic reaction can be indicated as follows:

$$M \rightarrow Me^{n+} + ne^- \quad (1)$$

The cathode reaction outside the pit can be expressed as follows:

$$O_2 + 2H_2O + 4e^- \rightarrow 4OH^- \quad (2)$$

Afterwards, metal ions produce secondary reaction as pH value increases [96]:

$$Me^{n+} + H_2O \rightarrow MeOH^{(n-1)+} + H^+ \quad (3)$$

$$2Me^{n+} + 2OH^- + H_2O \rightarrow 2MeOH^{(n-1)+} \quad (4)$$

These reactions induce sediment accumulating in the pit. The pH value outside the pit increases as the reaction progresses due to the production of OH^-. The sediment accumulation impedes the migration of ions both inward and outward the pit. Soluble salt in electrolyte, such as $Ca(HCO_3)_2$, turns into $CaCO_3$ sediment with the development of corrosion. Therefore, the accumulation of sediment would form occluded cells. Dissolved oxygen hardly diffuses into the pit after the formation of occluded cell. As such, oxygen concentration difference is formed between the inside and outside of pit. Outward diffusion of dissolved metal ions is also difficult, therefore the concentration of metal cations in the pit gradually increases. If the reaction takes place in the neutral solution containing Cl^-, Cl^- would transfer from outside to inside for keeping electrical neutrality. Therefore, the concentration of Cl^- rises inside the pit. As mentioned above, the environment with high-concentration Cl^- would accelerate the corrosion of metal. As corrosion progresses, more Cl^- migrate into pits, which further accelerates the corrosion of metal. Such a circulation behaves as an autocatalytic process until the formation of stable pitting.

2.2. Principle Influencing Factors of Pitting Corrosion

Applied potential.-Pitting potential is defined as the lowest potential which can result in the pitting phenomenon of metals in the passive state. As we know, the basic requirement of pitting corrosion for metals in the passive state is aggressive ions (such as Cl^- or Br^-) and dissolved oxygen in the electrolyte [96, 97]. Therefore, local corrosion is prone to take place when the applied potential is beyond a certain value [96]. In other words, the increase of potential enhances the driving force for the adsorption of aggressive ions [68]. The adsorption of aggressive ions causes the breakdown of passive film, which induces pitting corrosion of metals in the passive state. As such, the pitting potential also reflects the difficulty or the facility in the breakdown of passive film. Moreover, the existence of oxidant is prone to make the corrosion potential rise or even exceed a certain critical value-pitting potential (breakdown potential) [98]. Boucherit *et al.* [99] prepared solutions that respectively containing pitting agent, inhibitor and oxidant with different concentrations. Afterwards, they evaluated the performances of carbon steels in terms of the pitting potential and found that the oxidant promotes the efficiency of inhibitor. Therefore, the pitting corrosion of specific metals in specific environments can be examined according to the applied potential. Beck [100] drew a graph concerning the current densities of pitting corrosion for commercial pure Ti (CP–Ti) in 0.6 M KBr and 0.6 M HBr solutions as a function of applied potential. The results indicated that the current density of pitting corrosion increases linearly with the applied potential. Therefore, the increase of applied potential would facilitate pitting corrosion. Meanwhile, Beck [101] also potted a series of transient current density-potential curves for CP–Ti electrode in 1 M KBr. Metastable pits are found between 1 V and 1.5 V. When potential increases to about 3.8 V, stable pits are formed. Basame and White [102] obtained a similar conclusion by voltammetric response of Ti/TiO_2 in 0.05 M KI solution. There is a small current undulation at 7.0 V, which reveals the formation of metastable pits. Moreover, stable pits are formed at 7.8 V.

Temperature.-In general, the function of temperature (T) vs. corrosion current density (i_{corr}) of Ti and Ti alloys follows the Arrhenius relationship, which can be expressed as [103, 104]:

$$\log i_{corr} = \mathrm{C} - \frac{E_a}{2.3RT} \quad (5)$$

where C is a constant, E_a is activation energy and R is gas constant. Such an equation indicates that the corrosion current densities of Ti and Ti alloys increase with environment temperature. Therefore, the corrosion rate of Ti and Ti alloys increases exponentially with temperature. Like potential, temperature is also a critical factor of pitting corrosion. Stable pitting takes place over a specific temperature which is called critical pitting temperature (CPT). The initiation of metastable pits or the formation of stable pits hardly takes place at a low temperature [97]. Hence, only extremely high breakdown potential can observed at a low temperature for metallic materials, which is related to the transpassive dissolution instead of local corrosion [68]. Over CPT, pitting corrosion can take place at a potential which is far below the transpassive potential [68]. Therefore, CPT is an important index related to the transformation from metastable pits to stable pits [97]. Below CPT, alloys cannot maintain the anodic current density (the necessary condition for pitting corrosion) [97]. Liu *et al.* [105] plotted the current-temperature curve of Ti in 0.1 M Na_2SO_4 solution at a potential of 1.1 V and found that metastable pitting takes place from 128 °C, while the stable pitting takes place at 205 °C [105]. Burstein *et al*. [85] investigated the influence of temperature on the pitting nucleation of CP–Ti micro-electrode in Ringer's physiological solution. The frequency of breakdown remarkably increases with rising temperature, which means the occurrence of pitting corrosion [85].

Alloy compositions.-It is well known that the alloy compositions influence the pitting corrosion of metallic materials [68, 106, 107]. The addition of certain elements is beneficial for the properties of passive film, hence improving the pitting corrosion resistance [108]. However, the added elements would also produce crystallographic defects and distinct phases, which form galvanic couples and eventually cause pitting corrosion [108-110]. Some specific examples are used to intuitively understand the influence of alloy compositions on pitting corrosion. Oliveira *et al*. [111] investigated the corrosion resistance of Ti–50Zr and Ti–13Nb–13Zr alloys in various solutions. They found that the two alloys exhibit similar voltammetric responses and no transpassivation in solutions of H_2SO_4, HNO_3, CH_3SO_3H and H_3PO_4 (pH=1) are observed at the potential up to 8 V. Pitting corrosion of Ti–50Zr alloy takes place at a potential over 2 V in $HClO_4$, while Ti–13Nb–13Zr alloy remains excellent corrosion resistance at the potential up to 8 V under the same condition. Therefore, the contents of Nb and Zr lead to different pitting behavior of Ti–50Zr and Ti–13Nb–13Zr. Glass and Hong [112] immersed Ti–Mo alloys (the contents of Mo = 10, 20, 30 wt.%) in 1 M H_2SO_4, and found that the increased content of Mo improves the thermodynamic stability of Ti, which enhances the pitting corrosion resistance accordingly.

Other unclear factors.-The oxide layer plays a key role in protecting alloys from corrosion. However, the protective passive film would degrade in the acidic solutions, which encourages the corrosion rate [113]. Zhong *et al.* [114] found that the corrosion potential of Ti electrode increases from -665 mV to -402 mV in the electrolytes with different pH values from 2.8 to 9.8. Interestingly, the current density (1.08 ± 0.2 μA cm^{-2}) is the lowest at the pH of 7.0 as compared to those at other pH values, while the pitting potential (1501 mV) is the highest. By contrast, Sueptitz *et al.* [115], found that Ti–Fe–Sn alloys reveal low corrosion rate and high stability to pitting corrosion in a wide range of pH values. Similarly, Virtanen and Curty [116] considered pH values have little influence on the pitting corrosion of Ti. Such a contradiction was explained by Maria *et al.* [117], who investigated the pitting corrosion of Ti–6Al–4V and Ti–13Nb–13Zr alloys. The results showed that the pitting behavior of Ti–13Nb–13Zr alloy is sensitive to the change in pH value and Ti–6Al–4V alloy is insensitive in the electrolytes with different pH values. However, the pH value of body fluid is almost stable, which is a neutral salt environment at a temperature of ~37 ºC. Therefore, the effect of pH on corrosion of Ti and Ti alloys may be neglected in the human body unless some diseases take place (such as inflammation and infection) [118].

Furthermore, Beck [100] also put forward another factor, namely, flow rate of electrolyte. They immersed CP–Ti in flowing iodide solution, bromide solution and chloride solution, respectively. However, CP–Ti exhibit different behavior in these solutions. The pitting corrosion current density increases with flow rate in iodide solution but decreases with flow rate in bromide solution. In chloride solution, pitting corrosion is completely absent. Therefore, pitting corrosion behavior of CP–Ti varies with different solutions in flowing electrolyte. A hypothesis was supposed that pitting corrosion in iodide solution could be related to oxide accumulation. As such, flowing electrolyte removes the blocking oxide, leading to pitting corrosion [100]. By contrast, in bromide solution and chloride solution, the concentration of hydrolytic product determines the production of passive film. Therefore, increased flow rate of electrolyte contributes to reduction in the concentration of hydrolytic productions, thereby improving pitting corrosion resistance [100]. However, there is still not enough evidence to support this hypothesis. Similar to the effect of pH value, the effect of flowing electrolyte is still not clear.

3. PITTING CORROSION OF VARIOUS TYPES OF TI AND TI ALLOYS

3.1. α-type Ti Alloys

α-type Ti alloys (such as CP–Ti and/or those Ti alloys only contains a trace of β-stabilizers) primarily consist of α phase [119-121]. α-type Ti alloys can maintain their strength and creep resistance under the temperature of 600 °C. The mechanical properties of α-type Ti alloys more rely on their compositions as compared to those of (α+β)-type Ti and β-type Ti alloys [122, 123]. For instance, the oxygen contents and processing procedures of α-type Ti alloys have significant influence on their properties [47]. Oxygen is the primary interstitial elements for Ti and Ti alloys [124]. Therefore, oxygen content is conducive to the strength of Ti and Ti alloys. In addition, processing procedures also determine the crystallographic characteristics of Ti and Ti alloys, which is another factor influencing the properties of metallic materials [60, 125-133]. It is well known that α-type Ti alloys exhibit excellent corrosion resistance, good weldability and high creep resistance. Therefore, α-type Ti alloys can be applied in the oral environment and high-temperature environment.

Although α-type Ti alloys have excellent corrosion resistance, their performances would be weakened in aggressive environments due to corrosion, especially pitting corrosion. Such a phenomenon is unfavorable for Ti and Ti alloys used in biomedical fields. The following examples are used to better understand the pitting corrosion of α-type Ti alloys in various environments. Neville and Xu [134] immersed CP–Ti in three different solutions (*i.e*., the HCl solutions at pH of 4 and pH of 2 as well as HCl solution with the addition of 500 ppm NaCl at pH of 4, respectively). They found that the critical pitting temperature of CP–Ti would decrease with decreasing the pH value. Casilla *et al.* [135] immersed CP–Ti electrode in 1 M KBr and 0.05 M H_2SO_4 solutions and measured the voltammetric responses by electrochemical measurements. They obtained a function of the pitting potential and the thickness of passive film. The function indicated that the pitting potential of CP–Ti is proportional to the average thickness of passive film. Cheng *et al.* [136] observed a considerable number of pits on CP–Ti immersed in the fluoridated solutions, which specifies the adverse influence of fluoridated solutions on CP–Ti. As mentioned above, one can note that the pitting corrosion of α-type Ti alloys is influenced by the factors mentioned in Section 2.

Generally, α-type Ti alloys (as well as other types of Ti alloys) can form a passive film (mainly consist of TiO_2) with 1.5~10 nm thickness at room temperature [137]. This oxide layer provides excellent corrosion resistance in aqueous environments and possesses low electronic and low ion conductivities [137]. As mentioned earlier, halide ions are detrimental to passive film to some extent, thereby leading to pitting corrosion. Furthermore, α-type Ti alloys have a high solubility for hydrogen, which indicates that the passive film of α-type Ti alloys is sensitive to H+ [138]. H+ attacks passive film (TiO_2) and causes the hydrolyzation reaction as below:

$$TiO_2 + 4H^+ \rightarrow 2H_2O + Ti^{4+} \quad (6)$$

Therefore, the possibility of pitting corrosion would increase in the aqueous solutions at low pH value.

3.2. (α+β)-Type Ti Alloys

(α+β)-type Ti alloys are defined as dual-phase alloys and they have excellent mechanical properties and good structural stability [93, 139-142]. The mechanical performances of (α+β)-type Ti alloys can be adjusted their microstructures by heat treatment due to the existence of β phase [143-146]. Ti–6Al–4V is the most used (α+β)-type Ti alloy in biomedical applications [147-151]. However, Ti–6Al–4V has toxic elements of Al and V. Therefore, many other (α+β)-type Ti alloys, such as Ti–6Al–7Nb and Ti–5Al–2.5Fe, are gradually developed to be employed in biomedical fields [152]. Ti–6Al–7Nb is used in some medical device: fasteners, wires, femoral hip stems and screws [47]. Ti–5Al–2.5 Fe is also frequently applied in the hip prostheses and hip prosthesis heads [47].

(α+β)-type Ti alloys also possess good corrosion resistance in a variety of aqueous environments. However, pitting corrosion is frequently observed for (α+β)-type Ti alloys. Barranco *et al.* [153] prepared three Ti–6Al–4V alloys with different surface roughnesses by blasting and evaluated their pitting sensitivities after oxidation treatment. They found that the pitting sensitivity of blasted Ti–6Al–4V alloy increases as the surface roughness increases. As is known, the topography of passive film is determined by the topography of Ti substrate. Therefore, one can conclude that the pitting corrosion of Ti alloys is also influenced by their topographies. López *et al.* [154] oxidized Ti–6Al–7Nb, Ti–13Nb–13Zr and Ti–15Zr–4Nb in air at 750 °C ranging from 6 h to 48 h and then examined their pitting sensitivities in Hank's solution by cyclic voltammetry method. The result revealed that Ti–6Al–7Nb shows smaller loop area (as well lower pitting sensitivity) compared with other two alloys. On the other hand, these three oxidized alloys have better pitting corrosion resistance than the non-oxidized counterparts [155], which indicates that the pre-formed oxide layer enhances the protection against pitting corrosion. Simsek and Ozyurek [156] investigated the pitting corrosion of Ti–5Al–

2.5Fe and Ti–6Al–4V alloys in simulated body fluid. Ti–6Al–4V alloy shows duct-shaped pits along the grain boundaries, which is considered to be related to the dissolution of V-rich zones [156]. In comparison, the pits on the Ti–5Al–2.5Fe alloys are mainly presented in β-phase zones.

According to the above statements, it can be concluded that the pitting behavior of dual-phase Ti alloys depends on their chemical compositions to a great extent. The changes in the compositions of the oxide layer would promote the occurrence of pitting. Therefore, some surface treatments, such as oxidation and anodic treatment, can improve pitting corrosion resistance [69]. On the other hand, (α+β)-type Ti alloys have two different phases, which are prone to produce micro-galvanic effect. The dissolution of micro-anode accelerates the formation of passive film. As such, the passivation phenomenon is more obvious in (α+β)-type Ti alloys [157]. Meanwhile, it has been reported that the oxide formed on β phase is more stable than that formed on α phase [158]. Codaro *et al.* [159] investigated the influence of heat treatment on pitting corrosion of selective laser melted Ti–6Al–4V by statistical analysis. They discovered that pits are mainly located in the interface of α/β phases. In annealed condition, pits are spherical and hemispherical, which are deeper than those in samples treated by the other conditions. Nevertheless, Sherif *et al*. [160] studied the effect of annealing temperature on pitting corrosion of Ti–54M alloy and found that uniform corrosion resistance and pitting corrosion resistance can be obviously improved at the annealing temperature of 940 °C. Hence, the annealing conditions significantly influence the microstructures and, therefore the pitting corrosion of dual-phase Ti alloys. As such, the corrosion behavior of dual-phase Ti alloys is more complex than that of single-phase Ti alloys, especially pitting corrosion.

3.3. β-type Ti Alloys

In β-type Ti alloys, Nb, Ta, Zr, Mo and other β stabilizers are added as main alloying elements [29, 70, 161-165]. Hence, β-type Ti alloys are primarily composed of β phase [166-172]. Their strength can be enhanced by quenching and subsequently aging at the temperature of 450 °C~650 °C, which is attributed to the dispersion strengthening. As with other hexagonal materials, aging treatment produces α phase resulted from the transformation from β phase, [47, 173-178]. For instance, the tensile strength of Ti–10V–2Fe–3Al alloys exceeds 1200 MPa after heat-treated at 760 °C and subsequently aged at 500 °C for 8 h [179]. Meanwhile, β-type Ti alloys exhibit lower modulus as compared to α-type Ti alloys and (α+β)-type Ti alloys since β phase exhibits lower modulus than α phase [180-185]. So far, many β-type Ti alloys have been developed, such as Ti–12Mo–6Zr–2Fe, Ti–13Mo–7Zr–3Fe, Ti–15Mo–5Zr–3Al, Ti–14Nb–13Zr, Ti–35Nb–7Zr–5Ta, Ti–34Nb–9Zr–8Ta, Ti–15Mo, Ti–12Mo–5Ta, Ti–25Nb–3Fe, Ti–35Nb and so on [180, 186-192]. β-type Ti alloys have better biocompatibility as compared to (α+β)-type Ti alloys due to the absence of toxic elements of Al and V [47]. Due to the better corrosion resistance of β phase, β-type Ti alloys also possess better corrosion resistance than (α+β)-type Ti alloys [47]. Owing to their fascinating properties, β-type Ti alloys also are expected to be biomedical materials. Therefore, it is important to β-type Ti alloys that whether they have good pitting corrosion resistance or not. Oliveira *et al*. [193] found that β-type Ti–15Mo alloy reveals a typical valve-metal behavior *via* potentiodynamic polarization tests in Ringer's solution (NaCl 8.61 g l^{-1}, $CaCl_2$ 0.49 g l^{-1}, KCl 0.30 g l^{-1}). Oliveira *et al.* [111] also found that Ti–13Nb–13Zr and Ti–50Zr alloys show similar voltammetric responses with no evidence of pitting corrosion in acidic solutions, even at potentials up to 8 V. How-

Table 2. Pitting corrosion potential, corrosion potential and critical pitting temperature (CPT) of CP-Ti and some Ti alloys.

Alloy	Type	*E*p (VSCE)	*E*corr (VSCE)	CPT (°C)	Environment	Refs.
CP-Ti Grade 2	α	—	—	83.1	HCl solution (pH=4.0)	[134]
Ti5111	α	—	—	94.7	HCl solution (pH=4.0)	[134]
CP-Ti Grade 2	α	—	—	198.0	1M NaCl solution (pH=7.0)	[105]
Ti-6Al-4V	α+β	—	—	98.2	HCl solution (pH=4.0)	[134]
Ti-6Al-4V	α+β	—	—	86.0	3.5wt.% NaCl solution (pH=7.0)	[89]
Ti-6Al-4V	α+β	0.250	-0.45± 0.04	—	Phosphate buffered saline (pH=7.4)	[195]
Ti-6Al-4V	α+β	-0.180	-0.47± 0.02	—	Serum and Urine joint fluid (pH=8.0)	[195]
Ti-6Al-4V	α+β	-0.100	-0.44 ±0.05	—	Serum (pH=7.6)	[195]
Ti-6Al-4V	α+β	0.250	-0.40 ± 0.18	—	Urine (pH=6.6)	[195]
Ti-6Al-4V (selective laser melted)	α+β	8.13~8.45 (α′ phase)	—	70.0 (α′ phase)	3.5wt.% NaCl solution (pH=7.0)	[89]
Ti-13Nb-13Zr	β	—	0.11	—	Hank's solution (pH=7.4)	[154]
Ti-15Zr-4Nb	β	—	0.14	—	Hank's solution (pH=7.4)	[154]

ever, Ti–13Nb–13Zr retains corrosion resistance in chloride-containing solution, while Ti–50Zr alloy undergoes local corrosion (pitting corrosion) at the potential even lower than 2 V. Meisterjahn *et al*. [194] reported that the pitting corrosion potential of pure Zr is approximately 1.6 V. Therefore, it can be seen that the excessive addition of Zr in Ti alloy would result in the similar corrosion behavior to pure Zr [111]. It is also suggested that adding Zr in Ti alloys may facilitate pitting corrosion. Moreover, Meisterjahn *et al.* [194] examined the pitting corrosion potentials of as-cast and heat-treated Ti–50Zr alloys and found that heat treatment has a slight effect on the pitting corrosion behavior of Ti–50Zr alloys. Hence, one can conclude that the chemical compositions may play a more significant role in the pitting corrosion for β-type alloys.

Combined the statements in Section 3.1 and 3.2, β-type Ti alloys have the best pitting corrosion resistance among the three types Ti alloys. Satendra *et al.* [180] also demonstrated this result by cyclic polarization tests in Ringer's solution. They found the loop areas of the cyclic polarization curves for these three alloys following the order of Ti–15Mo < Ti–6Al–4V < CP–Ti. It is well known that the smaller the loop area, the better the pitting corrosion resistance and vice versa. However, this result cannot illustrate that all β-type Ti alloys would have similar pitting behavior. For a simple comparison, Table **2** lists the Pitting corrosion potential, corrosion potential and critical pitting temperature of CP-Ti and some different-typed Ti alloys.

β-type Ti alloys always have single phase and they generally exhibit higher pitting corrosion than dual-phase Ti alloys owing to the absence of galvanic coupling effect between different phases [196]. Shoesmith *et al.* [197] reported that the different film formation rates on α phase and β phase would induce the breakdown of passive film at α/β interface, resulting in the pitting corrosion of dual-phase Ti alloys. However, a single-phase microstructure of Ti alloys can be obtained by appropriate heat treatment for β-type Ti alloys, which also eliminates the galvanic coupling effect and further improves their corrosion resistance. For two types of single-phase alloys (*i.e.* α- and β-types of Ti alloys), it is well known that α phase dissolves faster than β phase in various environments [198]. Therefore, β-types Ti alloys generally possess better corrosion resistance than α-types Ti alloys. Meanwhile, due to the inappropriate processing procedure, α′ martensite phase may be produced in α-type of Ti alloys, which is considered as the potential source for pitting corrosion [199]. Therefore, β-type Ti alloys often have better pitting corrosion resistance than α-type Ti alloys.

CONCLUSION

This article introduces the pitting corrosion of three types (α-type, α+β-type and β-type) of biomedical Ti alloys, including pitting corrosion mechanism, influencing factors as well as pitting behavior. At first, the importance of Ti and Ti alloys in the applications of biomedical fields is illustrated. However, pitting corrosion is frequently found for Ti and Ti implants, which is significantly harmful to human body. Therefore, the investigation of pitting corrosion for Ti and Ti alloys is significant. Based on the formation of pitting, the growth stages of pitting corrosion are introduced and the main influencing factors of pitting corrosion (corrosive environment, applied potential, temperature and alloy compositions) are also specified in detail. Afterwards, the distinct pitting behavior for various types of Ti and Ti alloys are introduced. β-type Ti alloys are considered to have better pitting corrosion resistance as compared to α-type and α+β-type alloys.

There are many different opinions about the growth of pitting corrosion, which has no consensus, although some models or hypotheses have been proposed. It is interesting to note that the stage of metastable pitting has received more attentions. Many models were proposed to find the precursor sites of pits in order to better understand the pitting corrosion. Three types of Ti alloys exhibit excellent corrosion resistance in a variety of aqueous environments while pitting corrosion is still found. The influencing factors of pitting corrosion for three types of Ti alloys can still be attributed to corrosive environment, applied potential, temperature and alloy compositions. Considering these four influencing factors is an effective way to deep understand the pitting corrosion for Ti and Ti alloys. Some methods, such as heat treatment and surface treatment, have been used for Ti and Ti alloys to improve their corrosion resistance. As a result, pitting corrosion resistance of Ti and Ti alloys is correspondingly improved. Therefore, synthesizing a protective surface layer may be better for Ti and Ti alloys against pitting corrosion as compared to bare metal surface.

CONSENT FOR PUBLICATION

Not applicable.

FUNDING

The authors would like to acknowledge the financial support provided by Jiangsu Province six talent peaks project (XCL-117), open foundation of Guangxi Key Laboratory of Processing for Non-ferrous Metals and Featured Materials, Guangxi University (Grant No. 2020GXYSOF01), Natural Science Foundation of Jiangsu (Grant No. BK20201456).

CONFLICT OF INTEREST

The authors declare no conflict of interest financial or otherwise.

ACKNOWLEDGEMENTS

Declared none.

REFERENCES

[1] Geetha, M.; Singh, A.K.; Asokamani, R.; Gogia, A.K. Ti based biomaterials, the ultimate choice for orthopaedic implants- a review. *Prog. Mater. Sci.,* **2009**, *54*, 397-425. http://dx.doi.org/10.1016/j.pmatsci.2008.06.004

[2] Chai, L.; Chen, K.; Zhi, Y.; Murty, K.L.; Chen, L.Y.; Yang, Z. Nanotwins induced by pulsed laser and their hardening effect in a Zr alloy. *J. Alloys Compd.,* **2018**, *748*, 163-170. http://dx.doi.org/10.1016/j.jallcom.2018.03.126

[3] Zhang, L.C.; Klemm, D.; Eckert, J.; Hao, Y.L.; Sercombe, T.B. Manufacture by selective laser melting and mechanical behavior of a biomedical Ti-24Nb-4Zr-8Sn alloy. *Scr. Mater.,* **2011**, *65*, 21-24. http://dx.doi.org/10.1016/j.scriptamat.2011.03.024

[4] Yu, P.; Zhang, L.C.; Zhang, W.Y.; Das, J.; Kim, K.B.; Eckert, J. Interfacial reaction during the fabrication of Ni60Nb40 metallic

glass particles-reinforced Al based MMCs. *Mater. Sci. Eng. A,* **2007**, *444*, 206-213.
http://dx.doi.org/10.1016/j.msea.2006.08.077

[5] Liu, Y.; Li, S.; Hou, W.; Wang, S.; Hao, Y.; Yang, R.; Sercombe, T.B.; Zhang, L.C. Electron Beam Melted Beta-type Ti-24Nb-4Zr-8Sn Porous Structures With High Strength-to-Modulus Ratio. *J. Mater. Sci. Technol.,* **2016**, *32*, 505-508.
http://dx.doi.org/10.1016/j.jmst.2016.03.020

[6] Zhang, L.C.; Xu, J. Glass-forming ability of melt-spun multicomponent (Ti, Zr, Hf)–(Cu, Ni, Co)–Al alloys with equiatomic substitution. *J. Non-Cryst. Solids,* **2004**, *347*, 166-172.
http://dx.doi.org/10.1016/j.jnoncrysol.2004.09.007

[7] Yang, H.-Y.; Wang, Z.; Shu, S.-L.; Lu, J.-B. Effect of Ta addition on the microstructures and mechanical properties of *in situ* bi-phase (TiB2-TiCxNy)/(Ni-Ta) cermets. *Ceram. Int.,* **2019**, *45*, 4408-4417.
http://dx.doi.org/10.1016/j.ceramint.2018.11.118

[8] Zhang, L.C.; Shen, Z.Q.; Xu, J. Glass formation in a (Ti, Zr, Hf)–(Cu, Ni, Ag)–Al high-order alloy system by mechanical alloying. *J. Mater. Res.,* **2003**, *18*, 2141-2149.
http://dx.doi.org/10.1557/JMR.2003.0300

[9] Calin, M.; Zhang, L.C.; Eckert, J. Tailoring of microstructure and mechanical properties of a Ti-based bulk metallic glass-forming alloy. *Scr. Mater.,* **2007**, *57*, 1101-1104.
http://dx.doi.org/10.1016/j.scriptamat.2007.08.018

[10] Zhang, L.-C.; Kim, K.B.; Yu, P.; Zhang, W.Y.; Kunz, U.; Eckert, J. Amorphization in mechanically alloyed (Ti, Zr, Nb)-(Cu, Ni)-Al equiatomic alloys. *J. Alloys Compd.,* **2007**, *428*, 157-163.
http://dx.doi.org/10.1016/j.jallcom.2006.03.092

[11] Zhang, L.C.; Shen, Z.Q.; Xu, J. Mechanically milling-induced amorphization in Sn-containing Ti-based multicomponent alloy systems. *Mater. Sci. Eng. A,* **2005**, *394*, 204-209.
http://dx.doi.org/10.1016/j.msea.2004.11.051

[12] Zhang, L.C.; Xu, J.; Ma, E. Mechanically Alloyed Amorphous Ti50(Cu0.45Ni0.55)44–xAlxSi4B2 Alloys with Supercooled Liquid Region. *J. Mater. Res.,* **2002**, *17*, 1743-1749.
http://dx.doi.org/10.1557/JMR.2002.0258

[13] Zhang, L.-C.; Xu, J.; Eckert, J. Thermal stability and crystallization kinetics of mechanically alloyed TiC/Ti-based metallic glass matrix composite. *J. Appl. Phys.,* **2006**, *100,* 033514.
http://dx.doi.org/10.1063/1.2234535

[14] Milosev, I. Metallic materials for biomedical application: Labratory and clinical studies. *Pure Appl. Chem.,* **2011**, *83*, 309-324.
http://dx.doi.org/10.1351/PAC-CON-10-07-09

[15] Zhang, L.C.; Xu, J.; Ma, E. Consolidation and properties of ball-milled Ti50Cu18Ni22Al4Sn6 glassy alloy by equal channel angular extrusion. *Mater. Sci. Eng. A,* **2006**, *434*, 280-288.
http://dx.doi.org/10.1016/j.msea.2006.06.085

[16] Yang, C.; Kang, L.M.; Li, X.X.; Zhang, W.W.; Zhang, D.T.; Fu, Z.Q.; Li, Y.Y.; Zhang, L.C.; Lavernia, E.J. Bimodal titanium alloys with ultrafine lamellar eutectic structure fabricated by semi-solid sintering. *Acta Mater.,* **2017**, *132*, 491-502.
http://dx.doi.org/10.1016/j.actamat.2017.04.062

[17] Zhang, L.C.; Attar, H. Selective Laser Melting of Titanium Alloys and Titanium Matrix Composites for Biomedical Applications: A Review. *Adv. Eng. Mater.,* **2016**, *18*, 463-475.
http://dx.doi.org/10.1002/adem.201500419

[18] Li, Y.; Yang, C.; Zhao, H.; Qu, S.; Li, X.; Li, Y. New developments of Ti-based alloys for biomedical applications. *Materials (Basel),* **2014**, *7*(3), 1709-1800.
http://dx.doi.org/10.3390/ma7031709 PMID: 28788539

[19] Liu, L.H.; Yang, C.; Wang, F.; Qu, S.G.; Li, X.Q.; Zhang, W.W.; Li, Y.Y.; Zhang, L.C. Ultrafine grained Ti-based composites with ultrahigh strength and ductility achieved by equiaxing microstructure. *Mater. Des.,* **2015**, *79*, 1-5.
http://dx.doi.org/10.1016/j.matdes.2015.04.032

[20] Zhang, L.C.; Lu, H.B.; Mickel, C.; Eckert, J. Ductile ultrafine-grained Ti-based alloys with high yield strength. *Appl. Phys. Lett.,* **2007**, *91,* 051906.
http://dx.doi.org/10.1063/1.2766861

[21] Liu, Y.J.; Li, S.J.; Zhang, L.C.; Hao, Y.L.; Sercombe, T.B. Early plastic deformation behaviour and energy absorption in porous β-type biomedical titanium produced by selective laser melting. *Scr. Mater.,* **2018**, *153*, 99-103.
http://dx.doi.org/10.1016/j.scriptamat.2018.05.010

[22] Zhao, S.; Li, S.J.; Wang, S.G.; Hou, W.T.; Li, Y.; Zhang, L.C.; Hao, Y.L.; Yang, R.; Misra, R.D.K.K.; Murr, L.E. Compressive and fatigue behavior of functionally graded Ti-6Al-4V meshes fabricated by electron beam melting. *Acta Mater.,* **2018**, *150*, 1-15.
http://dx.doi.org/10.1016/j.actamat.2018.02.060

[23] Ma, T.F.; Zhou, X.; Du, Y.; Li, L.; Zhang, L.C.; Zhang, Y.S.; Zhang, P.X. High temperature deformation and microstructural evolution of core-shell structured titanium alloy. *J. Alloys Compd.,* **2019**, *775*, 316-321.
http://dx.doi.org/10.1016/j.jallcom.2018.10.101

[24] Abdel-Hady Gepreel, M.; Niinomi, M. Biocompatibility of Ti-alloys for long-term implantation. *J. Mech. Behav. Biomed. Mater.,* **2013**, *20*, 407-415.
http://dx.doi.org/10.1016/j.jmbbm.2012.11.014 PMID: 23507261

[25] Rabadia, C.D.; Liu, Y.J.; Wang, L.; Sun, H.; Zhang, L.C. Laves phase precipitation in Ti-Zr-Fe-Cr alloys with high strength and large plasticity. *Mater. Des.,* **2018**, *154*, 228-238.
http://dx.doi.org/10.1016/j.matdes.2018.05.035

[26] Carman, A.; Zhang, L.C.; Ivasishin, O.M.; Savvakin, D.G.; Matviychuk, M.V.; Pereloma, E.V. Role of alloying elements in microstructure evolution and alloying elements behaviour during sintering of a near-β titanium alloy. *Mater. Sci. Eng. A,* **2011**, *528*, 1686-1693.
http://dx.doi.org/10.1016/j.msea.2010.11.004

[27] Lu, H.Z.; Yang, C.; Luo, X.; Ma, H.W.; Song, B.; Li, Y.Y.; Zhang, L.C. Ultrahigh-performance TiNi shape memory alloy by 4D printing. *Mater. Sci. Eng. A,* **2019**, *763,* 138166.
http://dx.doi.org/10.1016/j.msea.2019.138166

[28] Liu, S.; Wang, J.L.L.; Ma, R.L.W.; Zhong, Y.; Lu, W.; Zhang, L.C. Superelastic behavior of *in-situ* eutectic-reaction manufactured high strength 3D porous NiTi-Nb scaffold. *Scr. Mater.,* **2020**, *181*, 121-126.
http://dx.doi.org/10.1016/j.scriptamat.2020.02.025

[29] Rabadia, C.D.; Liu, Y.J.; Zhao, C.H.; Wang, J.C.; Jawed, S.F.; Wang, L.Q.; Chen, L.Y.; Sun, H.; Zhang, L.C. Improved trade-off between strength and plasticity in titanium based metastable beta type Ti-Zr-Fe-Sn alloys. *Mater. Sci. Eng. A,* **2019**, *766,* 138340.
http://dx.doi.org/10.1016/j.msea.2019.138340

[30] Wang, L.; Wang, C.; Zhang, L-C.; Chen, L.; Lu, W.; Zhang, D. Phase transformation and deformation behavior of NiTi-Nb eutectic joined NiTi wires. *Sci. Rep.,* **2016**, *6*, 23905.
http://dx.doi.org/10.1038/srep23905 PMID: 27049025

[31] Zhang, Y.S.; Hu, J.J.; Zhang, W.; Yu, S.; Yu, Z.T.; Zhao, Y.Q.; Zhang, L.C. Discontinuous core-shell structured Ti-25Nb-3Mo-3Zr-2Sn alloy with high strength and good plasticity. *Mater. Charact.,* **2019**, *147*, 127-130.
http://dx.doi.org/10.1016/j.matchar.2018.10.021

[32] Chen, Y.; Zhang, J.; Dai, N.; Qin, P.; Attar, H.; Zhang, L-C. Corrosion behaviour of selective laser melted Ti-TiB biocomposite in simulated body fluid. *Electrochim. Acta,* **2017**, *232*, 89-97.
http://dx.doi.org/10.1016/j.electacta.2017.02.112

[33] Challis, V.J.; Roberts, A.P.; Grotowski, J.F.; Zhang, L.C.; Sercombe, T.B. Prototypes for bone implant scaffolds designed via topology optimization and manufactured by solid freeform fabrication. *Adv. Eng. Mater.,* **2010**, *12*(11), 1106-1110.
http://dx.doi.org/10.1002/adem.201000154

[34] Attar, H.; Prashanth, K.G.; Zhang, L.C.; Calin, M.; Okulov, I.V.; Scudino, S.; Yang, C.; Eckert, J.r. Effect of powder particle shape on the properties of in situ Ti-TiB composite materials produced by selective laser melting. *J. Mater. Sci. Technol.,* **2015**, *31*, 1001-1005.
http://dx.doi.org/10.1016/j.jmst.2015.08.007

[35] Liu, Y.J.; Liu, Z.; Jiang, Y.; Wang, G.W.; Yang, Y.; Zhang, L.C. Gradient in microstructure and mechanical property of selective laser melted AlSi10Mg. *J. Alloys Compd.,* **2018**, *735*, 1414-1421. http://dx.doi.org/10.1016/j.jallcom.2017.11.020

[36] Attar, H.; Löber, L.; Funk, A.; Calin, M.; Zhang, L.C.; Prashanth, K.G.; Scudino, S.; Zhang, Y.S.; Eckert, J. Mechanical behavior of porous commercially pure Ti and Ti-TiB composite materials manufactured by selective laser melting. *Mater. Sci. Eng. A,* **2015**, *625*, 350-356. http://dx.doi.org/10.1016/j.msea.2014.12.036

[37] Li, X.X.; Yang, C.; Chen, T.; Zhang, L.C.; Hayat, M.D.; Cao, P. Influence of powder shape on atomic diffusivity and resultant densification mechanisms during spark plasma sintering. *J. Alloys Compd.,* **2019**, *802*, 600-608. http://dx.doi.org/10.1016/j.jallcom.2019.06.176

[38] Menzies, K.L.; Jones, L. The impact of contact angle on the biocompatibility of biomaterials. *Optom. Vis. Sci.,* **2010**, *87*(6), 387-399. http://dx.doi.org/10.1097/OPX.0b013e3181da863e PMID: 20375749

[39] Kuroda, D.; Niinomi, M.; Morinaga, M.; Kato, Y.; Yashiro, T. Design and mechanical properties of new β type titanium alloys for implant materials. *Mater. Sci. Eng. A,* **1998**, *243*, 244-249 http://dx.doi.org/10.1016/S0921-5093(97)00808-3

[40] Yang, H.-Y.; Wang, Z.; Yue, X.; Ji, P.-J.; Shu, S.-L., Simultaneously improved strength and toughness of in situ bi-phased TiB_2-Ti(C,N)-Ni cermets by Mo addition. *J. Alloys Compd.* **2019**, *820*, 153068. https://doi.org/10.1016/j.ceramint.2018.11.118

[41] Li, Q.; Qiu, F.; Dong, B-X.; Gao, X.; Shu, S-L.; Yang, H-Y.; Jiang, Q-C. Processing, multiscale microstructure refinement and mechanical property enhancement of hypoeutectic Al–Si alloys *via in situ* bimodal-sized TiB_2 particles. *Mater. Sci. Eng. A,* **2020**, *777*(10), 139081. http://dx.doi.org/10.1016/j.msea.2020.139081

[42] Niinomi, M. Mechanical biocompatibilities of titanium alloys for biomedical applications. *J. Mech. Behav. Biomed. Mater.,* **2008**, *1*(1), 30-42. http://dx.doi.org/10.1016/j.jmbbm.2007.07.001 PMID: 19627769

[43] Yang, Y.; Zhan, J.B.; Sun, Z.Z.; Wang, H.L.; Lin, J.X.; Liu, Y.J.; Zhang, L.C. Evolution of functional properties realized by increasing laser scanning speed for the selective laser melting fabricated NiTi alloy. *J. Alloys Compd.,* **2019**, *804*, 220-229. http://dx.doi.org/10.1016/j.jallcom.2019.06.340

[44] Culleton, P.; Prendergast, P.J.; Taylor, D. Fatigue failure in the cement mantle of an artificial hip joint. *Clin. Mater.,* **1993**, *12*(2), 95-102. http://dx.doi.org/10.1016/0267-6605(93)90056-D PMID: 10148336

[45] Wang, J.F. Modelling Young's modulus for porous bones with microstructural variation and anisotropy. *J. Mater. Sci. Mater. Med.,* **2010**, *21*(2), 463-472. http://dx.doi.org/10.1007/s10856-009-3919-6 PMID: 19882305

[46] Sumner, D.R.; Turner, T.M.; Igloria, R.; Urban, R.M.; Galante, J.O. Functional adaptation and ingrowth of bone vary as a function of hip implant stiffness. *J. Biomech.,* **1998**, *31*(10), 909-917. http://dx.doi.org/10.1016/S0021-9290(98)00096-7 PMID: 9840756

[47] Zhang, L.C.; Chen, L.Y. A Review on Biomedical Titanium Alloys: Recent Progress and Prospect. *Adv. Eng. Mater.,* **2019**, *21*(4), 1801215. http://dx.doi.org/10.1002/adem.201801215

[48] Ren, D.; Zhang, H.; Liu, Y.; Li, S.; Jin, W.; Yang, R.; Zhang, L. Microstructure and properties of equiatomic Ti–Ni alloy fabricated by selective laser melting. *Mater. Sci. Eng. A,* **2020**, *771,* 138586. http://dx.doi.org/10.1016/j.msea.2019.138586

[49] Niinomi, M.; Nakai, M.; Hieda, J. Development of new metallic alloys for biomedical applications. *Acta Biomater.,* **2012**, *8*(11), 3888-3903. http://dx.doi.org/10.1016/j.actbio.2012.06.037 PMID: 22765961

[50] Bauer, S.; Schmuki, P.; von der Mark, K.; Park, J. Engineering biocompatible implant surfaces. *Prog. Mater. Sci.,* **2013**, *58*(3), 261-326. http://dx.doi.org/10.1016/j.pmatsci.2012.09.001

[51] Ziemniak, S.; Hanson, M. Corrosion behavior of 304 stainless steel in high temperature, hydrogenated water. *Corros. Sci.,* **2002**, *44*(10), 2209-2230. http://dx.doi.org/10.1016/S0010-938X(02)00004-5

[52] Niinomi, M. Recent metallic materials for biomedical applications. *Metall. Mater. Trans., A Phys. Metall. Mater. Sci.,* **2002**, *33*, 477-486. http://dx.doi.org/10.1007/s11661-002-0109-2

[53] Wang, L.; Xie, L.; Zhang, L-C.; Chen, L.; Ding, Z.; Lv, Y.; Zhang, W.; Lu, W.; Zhang, D. Microstructure evolution and superelasticity of layer-like NiTiNb porous metal prepared by eutectic reaction. *Acta Mater.,* **2018**, *143*, 214-226. http://dx.doi.org/10.1016/j.actamat.2017.10.021

[54] Liu, Y.; Ren, D.; Li, S.; Wang, H.; Zhang, L.; Sercombe, T. Enhanced fatigue characteristics of a topology-optimized porous titanium structure produced by selective laser melting. *Addit. Manuf.,* **2020**, *32,* 101060. http://dx.doi.org/10.1016/j.addma.2020.101060

[55] Qin, P.; Chen, Y.; Liu, Y.-J.; Zhang, J.; Chen, L.-Y.; Li, Y.; Zhang, X.; Cao, C.; Sun, H.; Zhang, L.-C. Resemblance in corrosion behavior of selective laser melted and traditional monolithic β Ti-24Nb-4Zr-8Sn alloy. *ACS Biomater. Sci. Eng.,* **2019**, *5*, 1141-1149. http://dx.doi.org/10.1021/acsbiomaterials.8b01341

[56] Wang, L.; Qu, J.; Chen, L.; Meng, Q.; Zhang, L.C.; Qin, J.; Zhang, D.; Lu, W. Investigation of deformation mechanisms in β-Type Ti-35Nb-2Ta-3Zr alloy *via* FSP leading to surface strengthening. *Metall. Mater. Trans., A Phys. Metall. Mater. Sci.,* **2015**, *46*, 4813-4818. http://dx.doi.org/10.1007/s11661-015-3089-8

[57] Hafeez, N.; Liu, J.; Wang, L.; Wei, D.; Tang, Y.; Lu, W.; Zhang, L.-C. Superelastic response of low-modulus porous beta-type Ti-35Nb-2Ta-3Zr alloy fabricated by laser powder bed fusion *Addit. Manuf,* **2020**, *34*, 101264.

[58] Rabadia, C.; Liu, Y.; Jawed, S.; Wang, L.; Sun, H.; Zhang, L. Deformation and toughness behavior of beta-type titanium alloys comprising C15 type Laves phase. *Mater. Today Sustain.,* **2020**, *9,* 100034. http://dx.doi.org/10.1016/j.mtsust.2020.100034

[59] Gonza'lez, J.E.G.; Mirza-Rosca, J.C. Study of the corrosion behavior of titanium and some of its alloys for biomedical and dental implant applications. *J. Electroanal. Chem. (Lausanne Switz.),* **1999**, *471*, 109-115. http://dx.doi.org/10.1016/S0022-0728(99)00260-0

[60] Chen, L.; Zeng, Q.; Li, J.; Lu, J.; Zhang, Y.; Zhang, L-C.; Qin, X.; Lu, W.; Zhang, L.; Wang, L.; Zhang, D. Effect of microstructure on corrosion behavior of a Zr-Sn-Nb-Fe-Cu-O alloy. *Mater. Des.,* **2016**, *92*, 888-896. http://dx.doi.org/10.1016/j.matdes.2015.12.067

[61] Chen, L.; Li, J.; Zhang, Y.; Zhang, L.C.; Lu, W.; Wang, L.; Zhang, L.; Zhang, D. Zr-Sn-Nb-Fe-Si-O alloy for fuel cladding candidate: Processing, microstructure, corrosion resistance and tensile behavior. *Corros. Sci.,* **2015**, *100*, 332-340. http://dx.doi.org/10.1016/j.corsci.2015.08.005

[62] Chen, L.Y.; Shen, P.; Zhang, L.; Lu, S.; Chai, L.; Yang, Z.; Zhang, L.C. Corrosion behavior of non-equilibrium Zr-Sn-Nb-Fe-Cu-O alloys in high-temperature 0.01 M LiOH aqueous solution and degradation of the surface oxide films. *Corros. Sci.,* **2018**, *136*, 221-230. http://dx.doi.org/10.1016/j.corsci.2018.03.012

[63] Tan, H.; Hu, T.; Wang, Y.; Zhang, F.; Qiu, Y.; Liu, T.; Fan, W.; Zhang, L.-C. Solidification effect on the microstructure and mechanism of laser solid forming produced flame-resistant Ti-35V-15Cr alloy. *Adv. Eng. Mater.,* **2020**, *22,* 20200102. http://dx.doi.org/10.1002/adem.202000102

[64] Xiang, K.; Chen, L.-Y.; Chai, L.; Guo, N.; Wang, H. Microstructural characteristics and properties of CoCrFeNiNbx high-entropy alloy coatings on pure titanium substrate by pulsed laser cladding. *Appl. Surf. Sci.,* **2020**, *517,* 146214. http://dx.doi.org/10.1016/j.apsusc.2020.146214

[65] Niinomi, M. Mechanical properties of biomedical titanium alloys. *Mater. Sci. Eng. A,* **1998**, *243*, 231-236. http://dx.doi.org/10.1016/S0921-5093(97)00806-X

[66] Macdonald, D.D. Passivity–the key to our metals-based civilization. *Pure Appl. Chem.,* **1999**, *71*, 951-978. http://dx.doi.org/10.1351/pac199971060951

[67] Jiang, Z.; Dai, X.; Norby, T.; Middleton, H. Investigation of pitting resistance of titanium based on a modified point defect model. *Corros. Sci.,* **2011**, *53*(2), 815-821. http://dx.doi.org/10.1016/j.corsci.2010.11.015

[68] Frankel, G.S. Pitting corrosion of metals a review of the critical factors. *J. Electrochem. Soc.,* **1998**, *145*(6), 2186-2198. http://dx.doi.org/10.1149/1.1838615

[69] Zhang, L-C.; Chen, L.-Y.; Wang, L. Surface modification of titanium and titanium alloys: technologies, developments and future interests. *Adv. Eng. Mater.,* **2020**, *22,* 1901258. http://dx.doi.org/10.1002/adem.201901258

[70] Liu, Y.J.; Zhang, Y.S.; Zhang, L.C. Transformation-induced plasticity and high strength in beta titanium alloy manufactured by selective laser melting. *Materialia,* **2019**, *6,* 100299. http://dx.doi.org/10.1016/j.mtla.2019.100299

[71] Zhang, Y.; Kent, D.; Wang, G.; St John, D.; Dargusch, M. An investigation of the mechanical behaviour of fine tubes fabricated from a Ti–25Nb–3Mo–3Zr–2Sn alloy. *Mater. Des.,* **2015**, *85*, 256-265. http://dx.doi.org/10.1016/j.matdes.2015.06.127

[72] Jirarungsatian, C.; Prateepasen, A. Pitting and uniform corrosion source recognition using acoustic emission parameters. *Corros. Sci.,* **2010**, *52*(1), 187-197. http://dx.doi.org/10.1016/j.corsci.2009.09.001

[73] Dai, N.; Wu, J.; Zhang, L.-C.; Yin, L.; Yang, Y.; Jiang, Y.; Li, J. Pitting and etching behaviors occurring in duplex stainless steel 2205 in the presence of alternating voltage interference. *Constr. Build. Mater.,* **2019**, *202*, 877-890. http://dx.doi.org/10.1016/j.conbuildmat.2019.01.084

[74] Dai, N.; Wu, J.; Zhang, L.C.; Sun, Y.; Liu, Y.; Yang, Y.; Jiang, Y.; Li, J. Alternating voltage induced oscillation on electrochemical behavior and pitting corrosion in duplex stainless steel 2205. *Mater. Corros.,* **2019**, *70*(3), 419-433. http://dx.doi.org/10.1002/maco.201810438

[75] Dai, N.; Wan, Y.; Liu, Y.; Sun, Y.; Zhang, L.C.; Jiang, Y.; Li, J. Studies on pitting corrosion in austenitic stainless steel interfered by square-wave alternating voltage with different parameters using multi-potential steps method. *Mater. Corros.,* **2018**, *69*(12), 1741-1757. http://dx.doi.org/10.1002/maco.201810199

[76] Burstein, G.T.; Liu, C. Nucleation of corrosion pits in Ringer's solution containing bovine serum. *Corros. Sci.,* **2007**, *49*(11), 4296-4306. http://dx.doi.org/10.1016/j.corsci.2007.05.018

[77] Szklarska-Smialowska, Z. Mechanism of pit nucleation by electrical breakdown of the passive film. *Corros. Sci.,* **2002**, *44*, 1143-1149. http://dx.doi.org/10.1016/S0010-938X(01)00113-5

[78] Stehblow, H.-H. Nucleation and repassivation of corrosion pits for pitting on iron and nickel. *Mater. Corros.,* **1976**, *27*, 792. http://dx.doi.org/10.1002/maco.19760271106

[79] Hoar, T.P.; Mears, D.C.; Rothwell, G.P. The relationships between anodic passivity, brightening and pitting. *Corros. Sci.,* **1965**, *5*, 279-289. http://dx.doi.org/10.1016/S0010-938X(65)90614-1

[80] Zhang, B.; Wang, J.; Wu, B.; Guo, X.W.; Wang, Y.J.; Chen, D.; Zhang, Y.C.; Du, K.; Oguzie, E.E.; Ma, X.L. Unmasking chloride attack on the passive film of metals. *Nat. Commun.,* **2018**, *9*(1), 2559. http://dx.doi.org/10.1038/s41467-018-04942-x PMID: 29967353

[81] Soltis, J. Passivity breakdown, pit initiation and propagation of pits in metallic materials- Review. *Corros. Sci.,* **2015**, *90*, 5-22. http://dx.doi.org/10.1016/j.corsci.2014.10.006

[82] Sato, N. A theory for breakdown of anodic oxide films on metals. *Electrochim. Acta,* **1971**, *16*, 1683-1692. http://dx.doi.org/10.1016/0013-4686(71)85079-X

[83] Hoar, T.P.; Jacob, W.R. Breakdown of passivity of stainless steel by halide ions. *Nature,* **1967**, *216*, 1299-1301. http://dx.doi.org/10.1038/2161299a0

[84] Jiang, Z.; Norby, T.; Middleton, H. Evaluation of metastable pitting on titanium by charge integration of current transients. *Corros. Sci.,* **2010**, *52*(10), 3158-3161. http://dx.doi.org/10.1016/j.corsci.2010.03.012

[85] Burstein, G.T.; Liu, C.; Souto, R.M. The effect of temperature on the nucleation of corrosion pits on titanium in Ringer's physiological solution. *Biomaterials,* **2005**, *26*(3), 245-256. http://dx.doi.org/10.1016/j.biomaterials.2004.02.023 PMID: 15262467

[86] Tian, W.; Du, N.; Li, S.; Chen, S.; Wu, Q. Metastable pitting corrosion of 304 stainless steel in 3.5% NaCl solution. *Corros. Sci.,* **2014**, *85*, 372-379. http://dx.doi.org/10.1016/j.corsci.2014.04.033

[87] Virtanen, S.; Curty, C. Metastable and stable pitting corrosion of titanium in halide solutions. *Corrosion,* **2004**, *60*(7), 643-649. http://dx.doi.org/10.5006/1.3287839

[88] Lu, H.; Zhang, L.; Gebert, A.; Schultz, L. Pitting corrosion of Cu–Zr metallic glasses in hydrochloric acid solutions. *J. Alloys Compd.,* **2008**, *462*(1-2), 60-67. http://dx.doi.org/10.1016/j.jallcom.2007.08.023

[89] Seo, D-I.; Lee, J-B. Corrosion characteristics of additive-manufactured Ti-6Al-4V using microdroplet cell and critical pitting temperature techniques. *J. Electrochem. Soc.,* **2019**, *166*(13), C428-C433. http://dx.doi.org/10.1149/2.0571913jes

[90] Laycock, N.J.; White, S.P. Computer Simulation of Single Pit Propagation. *J. Electrochem. Soc.,* **2001**, *148*, B264-B275. http://dx.doi.org/10.1149/1.1376119

[91] Jia, Z.; Lyu, F.; Zhang, L.; Zeng, S.; Liang, S.; Li, Y.; Lu, J. Pt nanoparticles decorated heterostructured gC_3N_4/Bi_2MoO_6 microplates with highly enhanced photocatalytic activities under visible light. *Sci. Rep.,* **2019**, *9*(1), 7636. http://dx.doi.org/10.1038/s41598-019-42973-6 PMID: 30626917

[92] Liang, S.-X.; Zhang, W.; Wang, W.; Jia, G.; Yang, W.; Zhang, L.-C. Surface reactivation of FeNiPC metallic glass: A strategy for highly enhanced catalytic behavior. *J. Phys. Chem. Solids,* **2019**, *132*, 89-98. http://dx.doi.org/10.1016/j.jpcs.2019.04.022

[93] Chen, Y.; Zhang, J.; Gu, X.; Dai, N.; Qin, P.; Zhang, L.C. Distinction of corrosion resistance of selective laser melted Al-12Si alloy on different planes. *J. Alloys Compd.,* **2018**, *747*, 648-658. http://dx.doi.org/10.1016/j.jallcom.2018.03.062

[94] Qin, P.; Liu, Y.; Sercombe, T.B.; Li, Y.; Zhang, C.; Cao, C.; Sun, H.; Zhang, L.-C. Improved corrosion resistance on selective laser melting produced Ti-5Cu alloy after heat treatment. *ACS Biomater. Sci. Eng.,* **2018**, *4*, 2633-2642. http://dx.doi.org/10.1021/acsbiomaterials.8b00319

[95] Guan, L.; Li, Y.; Wang, G.; Zhang, Y.; Zhang, L.C. pH dependent passivation behavior of niobium in acid fluoride-containing solutions. *Electrochim. Acta,* **2018**, *285*, 172-184. http://dx.doi.org/10.1016/j.electacta.2018.07.221

[96] Vermilye, D.A. Concerning the critical pitting potential. *J. Electrochem. Soc.,* **1971**, *118*, 529-531. http://dx.doi.org/10.1149/1.2408104

[97] Laycock, N.; Moayed, M.H.; Newman, R. Metastable pitting and the critical pitting temperature. *J. Electrochem. Soc.,* **1998**, *145*(8), 2622.
http://dx.doi.org/10.1149/1.1838691

[98] Man, H.C.; Gabe, D.R., The study of pitting potentials for some austenitic stainless steels using a potentiodynamic technique. *Corros. Sci.,* **1981**, *21*, 713-721.
http://dx.doi.org/10.1016/0010-938X(81)90018-4

[99] Boucherit, M.N.; Amzert, S.A.; Arbaoui, F.; Hanini, S.; Hammache, A. Pitting corrosion in presence of inhibitors and oxidants. *Anti-Corros. Methods Mater.,* **2008**, *55*(3), 115-122.
http://dx.doi.org/10.1108/00035590810870419

[100] Beck, T.R. Pitting of titanium I. Titaniumá foil experiments. *J. Electrochem. Soc.,* **1973**, *120*, 1310-1316.
http://dx.doi.org/10.1149/1.2403253

[101] Beck, T.R. Pitting of titanium II. One-dimensional pit experiments. *J. Electrochem. Soc.,* **1973**, *120*, 1317-1324.
http://dx.doi.org/10.1149/1.2403254

[102] Basame, S.B.; White, H.S. The relationship between pitting potential and competitive anion adsorption. *J. Electrochem. Soc.,* **2000**, *147*, 1376-1381.
http://dx.doi.org/10.1149/1.1393364

[103] Fekry, A. The influence of chloride and sulphate ions on the corrosion behavior of Ti and Ti-6Al-4V alloy in oxalic acid. *Electrochim. Acta,* **2009**, *54*(12), 3480-3489.
http://dx.doi.org/10.1016/j.electacta.2008.12.060

[104] Atapour, M.; Fathi, M.; Shamanian, M. Corrosion behavior of Ti–6Al–4V alloy weldment in hydrochloric acid. *Mater. Corros.,* **2012**, *63*(2), 134-139.
http://dx.doi.org/10.1002/maco.201005821

[105] Liu, J.; Alfantazi, A.; Asselin, E. Effects of Temperature and sulfate on the pitting corrosion of titanium in high-temperature chloride solutions. *J. Electrochem. Soc.,* **2015**, *162*(4), C189-C196.
http://dx.doi.org/10.1149/2.0541504jes

[106] Chen, L.; Li, J.; Zhang, Y.; Zhang, L.C.; Lu, W.; Zhang, L.; Wang, L.; Zhang, D. Effects of alloyed Si on the autoclave corrosion performance and periodic corrosion kinetics in Zr-Sn-Nb-Fe-O alloys. *Corros. Sci.,* **2015**, *100*, 651-662.
http://dx.doi.org/10.1016/j.corsci.2015.08.043

[107] Sang, P.; Chen, L.-Y.; Zhao, C.; Wang, Z.-X.; Wang, H.; Lu, S.; Song, D.; Xu, J.-H.; Zhang, L.-C. Particle size-dependent microstructure, hardness and electrochemical corrosion behavior of atmospheric plasma sprayed NiCrBSi coatings. *Metals (Basel),* **2019**, *9*(12), 1342.
http://dx.doi.org/10.3390/met9121342

[108] Fornell, J.; Pellicer, E.; Van Steenberge, N.; González, S.; Gebert, A.; Suriñach, S.; Baró, M.D.; Sort, J. Improved plasticity and corrosion behavior in Ti–Zr–Cu–Pd metallic glass with minor additions of Nb: An alloy composition intended for biomedical applications. *Mater. Sci. Eng. A,* **2013**, *559*, 159-164.
http://dx.doi.org/10.1016/j.msea.2012.08.058

[109] Geetha, M.; Kamachi Mudali, U.; Gogia, A.K.; Asokamani, R.; Raj, B. Influence of microstructure and alloying elements on corrosion behavior of Ti–13Nb–13Zr alloy. *Corros. Sci.,* **2004**, *46*(4), 877-892.
http://dx.doi.org/10.1016/S0010-938X(03)00186-0

[110] Wang, J.; Liang, S.; Jia, Z.; Zhang, W.; Wang, W.; Liu, Y.; Lu, J.; Zhang, L. Chemically dealloyed Fe-based metallic glass with void channels-like architecture for highly enhanced peroxymonosulfate activation in catalysis. *J. Alloys Compd.,* **2019**, *785*, 642-650.
http://dx.doi.org/10.1016/j.jallcom.2019.01.130

[111] Oliveira, N.T.C.; Ferreira, E.A.; Duarte, L.T.; Biaggio, S.R.; Rocha-Filho, R.C.; Bocchi, N. Corrosion resistance of anodic oxides on the Ti–50Zr and Ti–13Nb–13Zr alloys. *Electrochim. Acta,* **2006**, *51*(10), 2068-2075.
http://dx.doi.org/10.1016/j.electacta.2005.07.015

[112] Glass, R.S.; Hong, Y.K. Transpassive behaviour of titanium molybdenum alloys in 1 M H_2SO_4. *Electrochim. Acta,* **1984**, *29*, 1465-1470.
http://dx.doi.org/10.1016/0013-4686(84)87029-2

[113] Barão, V.A.; Mathew, M.T.; Assunção, W.G.; Yuan, J.C.; Wimmer, M.A.; Sukotjo, C. Stability of cp-Ti and Ti-6Al-4V alloy for dental implants as a function of saliva pH - an electrochemical study. *Clin. Oral Implants Res.,* **2012**, *23*(9), 1055-1062.
http://dx.doi.org/10.1111/j.1600-0501.2011.02265.x PMID: 22092540

[114] Zhong, Y.; Yang, Q.; Li, X.; Yao, F.; Xie, L.; Zhao, J.; Chen, F.; Xie, T.; Zeng, G. Electrochemically induced pitting corrosion of Ti anode: Application to the indirect reduction of bromate. *Chem. Eng. J.,* **2016**, *289*, 114-122.
http://dx.doi.org/10.1016/j.cej.2015.12.091

[115] Sueptitz, R.; Das, J.; Baunack, S.; Gebert, A.; Schultz, L.; Eckert, J. Corrosion and pitting behaviour of ultrafine eutectic Ti–Fe–Sn alloys. *J. Alloys Compd.,* **2010**, *503*(1), 19-24.
http://dx.doi.org/10.1016/j.jallcom.2010.05.052

[116] Virtanen, S.; Curty, C. Metastable and stable pitting corrosion of titanium in halide solutions. *Corrosion,* **2003**, *60*, 643-649.
http://dx.doi.org/10.5006/1.3287839

[117] Souza, M.E.; Lima, L.; Lima, C.R.; Zavaglia, C.A.; Freire, C.M. Effects of pH on the electrochemical behaviour of titanium alloys for implant applications. *J. Mater. Sci. Mater. Med.,* **2009**, *20*(2), 549-552.
http://dx.doi.org/10.1007/s10856-008-3623-y PMID: 18987951

[118] Renvert, S.; Roos-Jansåker, A.M.; Lindahl, C.; Renvert, H.; Rutger Persson, G. Infection at titanium implants with or without a clinical diagnosis of inflammation. *Clin. Oral Implants Res.,* **2007**, *18*(4), 509-516.
http://dx.doi.org/10.1111/j.1600-0501.2007.01378.x PMID: 17517058

[119] Zhang, L.-C.; Liu, Y.; Li, S.; Hao, Y. Additive manufacturing of titanium alloys by electron beam melting: A review. *Adv. Eng. Mater.,* **2018**, *20,* 1700842.
http://dx.doi.org/10.1002/adem.201700842

[120] Chen, P.; Liao, W.B.; Liu, L.H.; Luo, F.; Wu, X.Y.; Li, P.J.; Yang, C.; Yan, M.; Liu, Y.; Zhang, L.C.; Liu, Z.Y. Ultrafast consolidation of bulk nanocrystalline titanium alloy through ultrasonic vibration. *Sci. Rep.,* **2018**, *8*(1), 801.
http://dx.doi.org/10.1038/s41598-018-19190-8 PMID: 29335515

[121] Wen, Y.; Xie, L.; Wang, Z.; Wang, L.; Lu, W.; Zhang, L-C. Nanoindentation characterization on local plastic response of Ti-6Al-4V under high-load spherical indentation. *J. Mater. Res. Tech.,* **2019**, *8*(4), 3434-3442.
http://dx.doi.org/10.1016/j.jmrt.2019.06.009

[122] Zhang, Y.S.; Zhang, W.; Huo, W.T.; Hu, J.J.; Zhang, L.C. Microstructure, mechanical and wear properties of core–shell structural particle reinforced Ti-O alloys. *Vacuum,* **2017**, *139*, 44-50.
http://dx.doi.org/10.1016/j.vacuum.2017.02.006

[123] Zhang, Y.S.; Wang, X.; Zhang, W.; Huo, W.T.; Hu, J.J.; Zhang, L.C. Elevated tensile properties of Ti-O alloy with a novel core-shell structure. *Mater. Sci. Eng. A,* **2017**, *696*, 360-365.
http://dx.doi.org/10.1016/j.msea.2017.04.088

[124] Wei, Q.; Wang, L.; Fu, Y.; Qin, J.; Lu, W.; Zhang, D. Influence of oxygen content on microstructure and mechanical properties of Ti–Nb–Ta–Zr alloy. *Mater. Des.,* **2011**, *32*(5), 2934-2939.
http://dx.doi.org/10.1016/j.matdes.2010.11.049

[125] Qin, X.; Guo, X.; Lu, J.; Chen, L.; Qin, J.; Lu, W. Erosion-wear and intergranular corrosion resistance properties of AISI 304L austenitic stainless steel after low-temperature plasma nitriding. *J. Alloys Compd.,* **2017**, *698*, 1094-1101.
http://dx.doi.org/10.1016/j.jallcom.2016.12.164

[126] Chen, L.Y.; Xu, T.; Lu, S.; Wang, Z.X.; Chen, S.; Zhang, L.C. Improved hardness and wear resistance of plasma sprayed nanostructured NiCrBSi coating via short-time heat treatment. *Surf. Coat. Tech.,* **2018**, *350*, 436-444.

http://dx.doi.org/10.1016/j.surfcoat.2018.07.037

[127] Chen, L.; Li, J.; Zhang, Y.; Lu, W.; Zhang, L.C.; Wang, L.; Zhang, D. Effect of low-temperature pre-deformation on precipitation behavior and microstructure of a Zr-Sn-Nb-Fe-Cu-O alloy during fabrication. *J. Nucl. Sci. Technol.,* **2016**, *53*, 496-507. http://dx.doi.org/10.1080/00223131.2015.1059776

[128] Yang, Z.N.; Wang, X.B.; Liu, F.; Zhang, F.C.; Chai, L.J.; Qiu, R.S.; Chen, L.Y. Effect of intercritical annealing temperature on microstructure and mechanical properties of duplex Zr-2.5Nb alloy. *J. Alloys Compd.,* **2019**, *776*, 242-249. http://dx.doi.org/10.1016/j.jallcom.2018.10.320

[129] Zhang, M.; Li, Y.N.; Zhang, F.C.; Wang, X.B.; Chen, L.Y.; Yang, Z.N. Effect of annealing treatment on the microstructure and mechanical properties of a duplex Zr-2.5 Nb alloy. *Mater. Sci. Eng. A,* **2017**, *706*, 236-241. http://dx.doi.org/10.1016/j.msea.2017.08.107

[130] Chen, L.Y.; Sang, P.; Zhang, L.; Song, D.; Chu, Y.Q.; Chai, L.; Zhang, L.C. Homogenization and growth behavior of second-phase particles in a deformed Zr-Sn-Nb-Fe-Cu-Si-O alloy. *Metals (Basel),* **2018**, *8*, 759. http://dx.doi.org/10.3390/met8100759

[131] Zhang, L.; Chen, L.-Y.; Zhao, C.; Liu, Y.; Zhang, L.-C. Calculation of oxygen diffusion coefficients in oxide films formed on low-temperature annealed Zr alloys and their related corrosion behavior. *Metals,* **2019**, *9*, 850. http://dx.doi.org/10.3390/met9080850

[132] Zhang, Y.-M.; Chen, L.-Y.; Lu, S.; Zhao, C.; Wang, Y.-H. Refined microstructure and enhanced hardness in friction stir-welded AZ31 magnesium alloy induced by heat pipe with different cooling liquid. *Metals,* **2019**, *9*(11), 1227. http://dx.doi.org/10.3390/met9111227

[133] Guo, X.; Qian, C.; Wan, X.; Zhang, W.; Zhu, H.; Zhang, J.; Yang, H.; Lin, S.; Kong, Q.; Fan, T. Facile *in situ* fabrication of biomorphic Co_2P-Co_3O_4/rGO/C as an efficient electrocatalyst for the oxygen reduction reaction. *Nanoscale,* **2020**, *12*(7), 4374-4382. http://dx.doi.org/10.1039/C9NR10785A PMID: 32049080

[134] Neville, A.; Xu, J. An assessment of the instability of Ti and its alloys in acidic environments at elevated temperature. *J. Light Met.,* **2001**, *1*(2), 119-126. http://dx.doi.org/10.1016/S1471-5317(01)00005-0

[135] Casillas, N.; Charlebois, S.; Smyrl, W.H.; White, H.S. Pitting corrosion of titanium. *J. Electrochem. Soc.,* **1994**, *141*(3), 636-642. http://dx.doi.org/10.1149/1.2054783

[136] Cheng, Y.; Hu, J.; Zhang, C.; Wang, Z.; Hao, Y.; Gao, B. Corrosion behavior of novel Ti-24Nb-4Zr-7.9Sn alloy for dental implant applications in vitro. *J. Biomed. Mater. Res. B Appl. Biomater.,* **2013**, *101*(2), 287-294. http://dx.doi.org/10.1002/jbm.b.32838 PMID: 23166067

[137] Albayrak, Ç.; Alsaran, A. Corrosion behaviour after anodising of pre-nitrided CP-Ti. *Corros. Eng. Sci. Technol.,* **2013**, *46*(7), 807-811. http://dx.doi.org/10.1179/147842211X13094269889371

[138] Mccracken, G.M.; Maple, J.H.C. The trapping of hydrogen ions in molybdenum, titanium, tantalum and zirconium. *Br. J. Appl. Phys.,* **1967**, *18*, 919-930. http://dx.doi.org/10.1088/0508-3443/18/7/306

[139] Bai, Y.; Gai, X.; Li, S.; Zhang, L.-C.; Liu, Y.; Hao, Y.; Zhang, X.; Yang, R.; Gao, Y. Improved corrosion behaviour of electron beam melted Ti-6Al–4V alloy in phosphate buffered saline. *Corros. Sci.,* **2017**, *123*, 289-296. http://dx.doi.org/10.1016/j.corsci.2017.05.003

[140] Yang, C.; Zhu, M.D.; Luo, X.; Liu, L.H.; Zhang, W.W.; Long, Y.; Xiao, Z.Y.; Fu, Z.Q.; Zhang, L.C.; Lavernia, E.J. Influence of powder properties on densification mechanism during spark plasma sintering. *Scr. Mater.,* **2017**, *139*, 96-99. http://dx.doi.org/10.1016/j.scriptamat.2017.06.034

[141] Ding, Z.; Zhang, C.; Xie, L.; Zhang, L.-C.; Wang, L.; Lu, W. Effects of friction stir processing on the phase transformation and microstructure of TiO_2-compounded Ti-6Al-4V alloy. *Metall. Mater. Trans., A Phys. Metall. Mater. Sci.,* **2016**, *47*, 5675-5679. http://dx.doi.org/10.1007/s11661-016-3809-8

[142] Yuan, W.; Hou, W.; Li, S.; Hao, Y.; Yang, R.; Zhang, L.-C.; Zhu, Y. Heat treatment enhancing the compressive fatigue properties of open-cellular Ti-6Al-4V alloy prototypes fabricated by electron beam melting. *J. Mater. Sci. Technol.,* **2018**, *34*, 1127-1131. http://dx.doi.org/10.1016/j.jmst.2017.12.003

[143] Zhang, C.; Ding, Z.; Xie, L.; Zhang, L.C.; Wu, L.; Fu, Y.; Wang, L.; Lu, W. Electrochemical and *in vitro* behavior of the nanosized composites of Ti-6Al-4V and TiO_2 fabricated by friction stir process. *Appl. Surf. Sci.,* **2017**, *423*, 331-339. http://dx.doi.org/10.1016/j.apsusc.2017.06.141

[144] Zhou, X.; Ma, T.; Zhang, L.; Zhang, Y.; Zhang, P. Mechanical property and microstructure evolution of nitrogen-modified Ti-6Al-4V alloy with core-shell structure by hot compression. *Mater. Charact.,* **2018**, *142*, 270-275. http://dx.doi.org/10.1016/j.matchar.2018.05.051

[145] Liang, S.-X.; Wang, X.; Zhang, W.; Liu, Y.-J.; Wang, W.; Zhang, L.-C. Selective laser melting manufactured porous Fe-based metallic glass matrix composite with remarkable catalytic activity and reusability. *Appl. Mater. Today,* **2020**, *19,* 100543. http://dx.doi.org/10.1016/j.apmt.2019.100543

[146] Xie, L.; Liu, C.; Song, Y.; Guo, H.; Wang, Z.; Hua, L.; Wang, L.; Zhang, L.-C. Evaluation of microstructure variation of TC11 alloy after electroshocking treatment. *J. Mater. Res. Tech,* **2020**, *9*(2), 2455-2466.

[147] Dai, N.; Zhang, L.-C.; Zhang, J.; Zhang, X.; Ni, Q.; Chen, Y.; Wu, M.; Yang, C. Distinction in corrosion resistance of selective laser melted Ti-6Al-4V alloy on different planes. *Corros. Sci.,* **2016**, *111*, 703-710. http://dx.doi.org/10.1016/j.corsci.2016.06.009

[148] Dai, N.; Zhang, J.; Chen, Y.; Zhang, L.-C. Heat treatment degrading the corrosion resistance of selective laser melted Ti-6Al-4V alloy. *J. Electrochem. Soc.,* **2017**, *164*, C428-C434. http://dx.doi.org/10.1149/2.1481707jes

[149] Zhang, L.C.; Jia, Z.; Lyu, F.; Liang, S.X.; Lu, J. A review of catalytic performance of metallic glasses in wastewater treatment: Recent progress and prospects. *Prog. Mater. Sci.,* **2019**, *105,* 100576. http://dx.doi.org/10.1016/j.pmatsci.2019.100576

[150] Xie, L.; Wang, L.; Wang, K.; Yin, G.; Fu, Y.; Zhang, D.; Lu, W.; Hua, L.; Zhang, L.-C. TEM characterization on microstructure of Ti–6Al–4V/Ag nanocomposite formed by friction stir processing. *Materialia,* **2018**, *3*, 139-144. http://dx.doi.org/10.1016/j.mtla.2018.08.007

[151] Zhang, Y.S.; Hu, J.J.; Zhao, Y.Q.; Bai, X.F.; Huo, W.T.; Zhang, W.; Zhang, L.C. Microstructure and mechanical properties of a high-oxygen core-shell network structured Ti6Al4V alloy. *Vacuum,* **2018**, *149*, 140-145. http://dx.doi.org/10.1016/j.vacuum.2017.12.036

[152] Choubey, A.; Balasubramaniam, R.; Basu, B. Effect of replacement of V by Nb and Fe on the electrochemical and corrosion behavior of Ti–6Al–4V in simulated physiological environment. *J. Alloys Compd.,* **2004**, *381*, 288-294. http://dx.doi.org/10.1016/j.jallcom.2004.03.096

[153] Barranco, V.; Onofre, E.; Escudero, M.L.; García-Alonso, M.C. Characterization of roughness and pitting corrosion of surfaces modified by blasting and thermal oxidation. *Surf. Coat. Tech.,* **2010**, *204*(23), 3783-3793. http://dx.doi.org/10.1016/j.surfcoat.2010.04.051

[154] López, M.F.; Jiménez, J.A.; Gutiérrez, A. Corrosion study of surface-modified vanadium-free titanium alloys. *Electrochim. Acta,* **2003**, *48*(10), 1395-1401. http://dx.doi.org/10.1016/S0013-4686(03)00006-9

[155] López, M.F.; Gutiérrez, A.; Jiménez, J.A. In vitro corrosion behaviour of titanium alloys without vanadium. *Electrochim. Acta,* **2002**, *47*, 1359-1364. http://dx.doi.org/10.1016/S0013-4686(01)00860-X

[156] Simsek, I.; Ozyurek, D. Investigation of the wear and corrosion behaviors of Ti_5Al_2.5Fe and Ti_6Al_4V alloys produced by mechanical alloying method in simulated body fluid environment. *Mater. Sci. Eng. C,* **2019**, *94*, 357-363. http://dx.doi.org/10.1016/j.msec.2018.09.047 PMID: 30423718

[157] Tamilselvi, S.; Raman, V.; Rajendran, N. Corrosion behaviour of Ti–6Al–7Nb and Ti–6Al–4V ELI alloys in the simulated body fluid solution by electrochemical impedance spectroscopy. *Electrochim. Acta,* **2006**, *52*(3), 839-846. http://dx.doi.org/10.1016/j.electacta.2006.06.018

[158] Chen, J.-R.; Tsai, W.-T. *In situ* corrosion monitoring of Ti–6Al–4V alloy in H_2SO_4/HCl mixed solution using electrochemical AFM. *Electrochim. Acta,* **2011**, *56*(4), 1746-1751. http://dx.doi.org/10.1016/j.electacta.2010.10.024

[159] Codaro, E.N.; Nakazato, R.Z.; Horovistiz, A.L.; Ribeiro, L.M.F.; Ribeiro, R.B.; Hein, L.R.O. An image analysis study of pit formation on Ti–6Al–4V. *Mater. Sci. Eng. A,* **2003**, *341*(1-2), 202-210. http://dx.doi.org/10.1016/S0921-5093(02)00218-6

[160] Sherif, E-S.; El Danaf, E.; Abdo, H.; Zein El Abedin, S.; Al-Khazraji, H. Effect of annealing temperature on the corrosion protection of hot swaged Ti-54M alloy in 2 M HCl pickling solutions. *Metals,* **2017**, *7*(1). http://dx.doi.org/10.3390/met7010029

[161] Wang, L.; Xie, L.; Lv, Y.; Zhang, L.-C.; Chen, L.; Meng, Q.; Qu, J.; Zhang, D.; Lu, W. Microstructure evolution and superelastic behavior in Ti-35Nb-2Ta-3Zr alloy processed by friction stir processing. *Acta Mater.,* **2017**, *131*, 499-510. http://dx.doi.org/10.1016/j.actamat.2017.03.079

[162] Rabadia, C.D.; Liu, Y.J.; Chen, L.Y.; Jawed, S.F.; Wang, L.Q.; Sun, H.; Zhang, L.C. Deformation and strength characteristics of Laves phases in titanium alloys. *Mater. Des.,* **2019**, *179,* 107891. http://dx.doi.org/10.1016/j.matdes.2019.107891

[163] Chai, L.; Xia, J.; Zhi, Y.; Gou, Y.; Chen, L.; Yang, Z.; Guo, N. Deformation mode-determined misorientation and microstructural characteristics in rolled pure Zr sheet. *Sci. China Technol. Sci.,* **2018**, *61*, 1346-1352. http://dx.doi.org/10.1007/s11431-018-9292-1

[164] Liu, Y.J.; Wang, H.L.; Li, S.J.; Wang, S.G.; Wang, W.J.; Hou, W.T.; Hao, Y.L.; Yang, R.; Zhang, L.C. Compressive and fatigue behavior of beta-type titanium porous structures fabricated by electron beam melting. *Acta Mater.,* **2017**, *126*, 58-66. http://dx.doi.org/10.1016/j.actamat.2016.12.052

[165] Liu, Y.J.; Li, S.J.; Wang, H.L.; Hou, W.T.; Hao, Y.L.; Yang, R.; Sercombe, T.B.; Zhang, L.C. Microstructure, defects and mechanical behavior of beta-type titanium porous structures manufactured by electron beam melting and selective laser melting. *Acta Mater.,* **2016**, *113*, 56-67. http://dx.doi.org/10.1016/j.actamat.2016.04.029

[166] Ehtemam-Haghighi, S.; Liu, Y.; Cao, G.; Zhang, L.C. Phase transition, microstructural evolution and mechanical properties of Ti-Nb-Fe alloys induced by Fe addition. *Mater. Des.,* **2016**, *97*, 279-286. http://dx.doi.org/10.1016/j.matdes.2016.02.094

[167] Haghighi, S.E.; Lu, H.B.; Jian, G.Y.; Cao, G.H.; Habibi, D.; Zhang, L.C. Effect of α ″martensite on the microstructure and mechanical properties of beta-type Ti–Fe–Ta alloys. *Mater. Des.,* **2015**, *76*, 47-54. http://dx.doi.org/10.1016/j.matdes.2015.03.028

[168] Ehtemam-Haghighi, S.; Prashanth, K.G.; Attar, H.; Chaubey, A.K.; Cao, G.H.; Zhang, L.C. Evaluation of mechanical and wear properties of Ti-xNb-7Fe alloys designed for biomedical applications. *Mater. Des.,* **2016**, *111*, 592-599. http://dx.doi.org/10.1016/j.matdes.2016.09.029

[169] Liu, Y.J.; Li, X.P.; Zhang, L.C.; Sercombe, T.B. Processing and properties of topologically optimised biomedical Ti-24Nb-4Zr-8Sn scaffolds manufactured by selective laser melting. *Mater. Sci. Eng. A,* **2015**, *642*, 268-278. http://dx.doi.org/10.1016/j.msea.2015.06.088

[170] Zhang, L.C.; Das, J.; Lu, H.B.; Duhamel, C.; Calin, M.; Eckert, J. High strength Ti-Fe-Sn ultrafine composites with large plasticity. *Scr. Mater.,* **2007**, *57*, 101-104. http://dx.doi.org/10.1016/j.scriptamat.2007.03.031

[171] Liang, S.X.; Jia, Z.; Liu, Y.J.; Zhang, W.; Wang, W.; Lu, J.; Zhang, L.C. Compelling rejuvenated catalytic performance in metallic glasses. *Adv. Mater.,* **2018**, *30*(45), e1802764. http://dx.doi.org/10.1002/adma.201802764 PMID: 30277608

[172] Hafeez, N.; Liu, S.; Lu, E.; Wang, L.; Liu, R. lu, W.; Zhang, L. C., Mechanical behavior and phase transformation of β-type Ti-35Nb-2Ta-3Zr alloy fabricated by 3D-Printing. *J. Alloys Compd.,* **2019**, *790*, 117-126. http://dx.doi.org/10.1016/j.jallcom.2019.03.138

[173] Chai, L.J.; Wang, S.Y.; Wu, H.; Guo, N.; Pan, H.C.; Chen, L.Y.; Murty, K.L.; Song, B. α→β Transformation characteristics revealed by pulsed laser-induced non-equilibrium microstructures in duplex-phase Zr alloy. *Sci. China Technol. Sci.,* **2017**, *60*, 1255-1262. http://dx.doi.org/10.1007/s11431-016-9038-y

[174] Chen, K.; Zeng, L.; Li, Z.; Chai, L.; Wang, Y.; Chen, L-Y.; Yu, H. Effects of laser surface alloying with Cr on microstructure and hardness of commercial purity Zr. *J. Alloys Compd.,* **2019**, *784*, 1106-1112. http://dx.doi.org/10.1016/j.jallcom.2019.01.097

[175] Chai, L.; Wang, T.; Ren, Y.; Song, B.; Guo, N.; Chen, L. Microstructural and textural differences induced by water and furnace cooling in commercially pure Zr annealed in the α + β region. *Met. Mater. Int.,* **2018**, *24*, 673-680. http://dx.doi.org/10.1007/s12540-018-0079-6

[176] Ehtemam-Haghighi, S.; Liu, Y.; Cao, G.; Zhang, L.-C. Influence of Nb on the β→α″ martensitic phase transformation and properties of the newly designed Ti-Fe-Nb alloys. *Mater. Sci. Eng. C,* **2016**, *60*, 503-510. http://dx.doi.org/10.1016/j.msec.2015.11.072 PMID: 26706557

[177] Rabadia, C.D.; Liu, Y.J.; Jawed, S.F.; Wang, L.; Li, Y.H.; Zhang, X.H.; Sercombe, T.B.; Sun, H.; Zhang, L.C. Improved deformation behavior in Ti-Zr-Fe-Mn alloys comprising the C14 type Laves and β phases. *Mater. Des.,* **2018**, *160*, 1059-1070. http://dx.doi.org/10.1016/j.matdes.2018.10.049

[178] Ran, R.; Liu, Y.; Wang, L.; Lu, E.; Xie, L.; Lu, W.; Wang, K.; Zhang, L.-C. α ″Martensite and amorphous phase transformation mechanism in TiNbTaZr alloy incorporated with TiO_2 particles during friction stir processing. *Metall. Mater. Trans., A Phys. Metall. Mater. Sci.,* **2018**, *49*(6), 1986-1991. http://dx.doi.org/10.1007/s11661-018-4577-4

[179] Raghunathan, S.L.; Stapleton, A.M.; Dashwood, R.J.; Jackson, M.; Dye, D. Micromechanics of Ti–10V–2Fe–3Al: *In situ* synchrotron characterisation and modelling. *Acta Mater.,* **2007**, *55*(20), 6861-6872. http://dx.doi.org/10.1016/j.actamat.2007.08.049

[180] Kumar, S.; Sankara Narayanan, T.S.N. Electrochemical characterization of β-Ti alloy in Ringer's solution for implant application. *J. Alloys Compd.,* **2009**, *479*(1-2), 699-703. http://dx.doi.org/10.1016/j.jallcom.2009.01.036

[181] Yang, Y.; Li, G.P.; Wang, H.; Wu, S.Q.; Zhang, L.C.; Li, Y.L.; Yang, K. Formation of zigzag-shaped {112} 〈111〉 β mechanical twins in Ti-24.5Nb-0.7Ta-2Zr-1.4O alloy. *Scr. Mater.,* **2012**, *66*, 211-214. http://dx.doi.org/10.1016/j.scriptamat.2011.10.031

[182] Jawed, S.F.; Rabadia, C.D.; Liu, Y.J.; Wang, L.Q.; Li, Y.H.; Zhang, X.H.; Zhang, L.C. Beta-type Ti-Nb-Zr-Cr alloys with large plasticity and significant strain hardening. *Mater. Des.,* **2019**, *181,* 108064. http://dx.doi.org/10.1016/j.matdes.2019.108064

[183] Lu, S.; Ma, F.; Liu, P.; Li, W.; Liu, X.; Chen, X.; Zhang, K.; Han, Q.; Zhang, L.-C. Recrystallization behavior and super-elasticity of a metastable β-Type Ti-21Nb-7Mo-4Sn alloy during cold rolling and annealing. *J. Mater. Eng. Perform.,* **2018**, *27*(8), 4100-4106. http://dx.doi.org/10.1007/s11665-018-3476-6

[184] Jawed, S.F.; Rabadia, C.D.; Liu, Y.J.; Wang, L.Q.; Qin, P.; Li, Y.H.; Zhang, X.H.; Zhang, L.C. Strengthening mechanism and corrosion resistance of beta-type Ti-Nb-Zr-Mn alloys. *Mater. Sci. Eng. C,* **2020**, *110,* 110728.
http://dx.doi.org/10.1016/j.msec.2020.110728 PMID: 32204038

[185] Xie, L.; Guo, H.; Song, Y.; Liu, C.; Wang, Z.; Hua, L.; Wang, L.; Zhang, L.-C. Effects of electroshock treatment on microstructure evolution and texture distribution of near-β titanium alloy manufactured by directed energy deposition. *Mater. Charact.,* **2020**, *161,* 110137.
http://dx.doi.org/10.1016/j.matchar.2020.110137

[186] Chen, L.-Y.; Wang, H.; Zhao, C.; Lu, S.; Wang, Z.-X.; Sha, J.; Chen, S.; Zhang, L.-C. Automatic remelting and enhanced mechanical performance of a plasma sprayed NiCrBSi coating. *Surf. Coat. Tech.,* **2019**, *369*, 31-43.
http://dx.doi.org/10.1016/j.surfcoat.2019.04.052

[187] Chen, L.-Y.; Xu, T.; Wang, H.; Sang, P.; Lu, S.; Wang, Z.-X.; Chen, S.; Zhang, L.-C. Phase interaction induced texture in a plasma sprayed-remelted NiCrBSi coating during solidification: An electron backscatter diffraction study. *Surf. Coat. Tech.,* **2019**, *358*, 467-480.
http://dx.doi.org/10.1016/j.surfcoat.2018.11.019

[188] Rabadia, C.D.; Liu, Y.J.; Cao, G.H.; Li, Y.H.; Zhang, C.W.; Sercombe, T.B.; Sun, H.; Zhang, L.C. High-strength β stabilized Ti-Nb-Fe-Cr alloys with large plasticity. *Mater. Sci. Eng. A,* **2018**, *732*, 368-377.
http://dx.doi.org/10.1016/j.msea.2018.07.031

[189] Lei, X.; Dong, L.; Zhang, Z.; Liu, Y.; Hao, Y.; Yang, R.; Zhang, L-C. Microstructure, texture evolution and mechanical properties of VT3-1 titanium alloy processed by multi-pass drawing and subsequent isothermal annealing. *Metals,* **2017**, *7*, 131.
http://dx.doi.org/10.3390/met7040131

[190] Jawed, S.F.; Rabadia, C.D.; Liu, Y.J.; Wang, L.Q.; Li, Y.H.; Zhang, X.H.; Zhang, L.C. Mechanical characterization and deformation behavior of β-stabilized Ti-Nb-Sn-Cr alloys. *J. Alloys Compd.,* **2019**, *792*, 684-693.
http://dx.doi.org/10.1016/j.jallcom.2019.04.079

[191] Wang, J.; Liu, Y.; Qin, P.; Liang, S.; Sercombe, T.; Zhang, L. Selective laser melting of Ti–35Nb composite from elemental powder mixture: Microstructure, mechanical behavior and corrosion behavior. *Mater. Sci. Eng. A,* **2019**, *760*, 214-224.
http://dx.doi.org/10.1016/j.msea.2019.06.001

[192] Chen, J.; Ma, F.; Liu, P.; Liu, X.; Li, W.; Chen, X.; Zhang, K.; Zhang, L-C. Effects of different processing conditions on superelasticity and low modulus properties of metastable β-type Ti-35Nb-2Ta-3Zr alloy. *Vacuum,* **2017**, *146*, 164-169.
http://dx.doi.org/10.1016/j.vacuum.2017.09.047

[193] Oliveira, N.T.; Guastaldi, A.C. Electrochemical stability and corrosion resistance of Ti-Mo alloys for biomedical applications. *Acta Biomater.,* **2009**, *5*(1), 399-405.
http://dx.doi.org/10.1016/j.actbio.2008.07.010 PMID: 18707926

[194] Meisterjahn, P.; Hoppe, H.W.; Schultze, J.W. Electrochemical and XPS measurements on thin oxide films on zirconium. *J. Electroanal. Chem. Int. Electronchem.,* **1987**, *217*, 159-185.
http://dx.doi.org/10.1016/0022-0728(87)85072-6

[195] Hsu, R.W.-W.; Yang, C.-C.; Huang, C.-A.; Chen, Y.-S. Investigation on the corrosion behavior of Ti–6Al–4V implant alloy by electrochemical techniques. *Mater. Chem. Phys.,* **2004**, *86*(2-3), 269-278.
http://dx.doi.org/10.1016/j.matchemphys.2004.02.025

[196] Chen, L.-Y.; Cui, Y.-W.; Zhang, L.-C. Recent development in beta titanium alloys for biomedical applications. *Metals,* **2020**, *10*(9), 1139.
http://dx.doi.org/10.3390/met10091139

[197] He, X.; Noël, J.J.; Shoesmith, D.W. Effects of iron content on microstructure and crevice corrosion of grade-2 titanium. *Corrosion,* **2004**, *60*(4), 378-386.
http://dx.doi.org/10.5006/1.3287747

[198] Garfias-Mesias, L.; Smyrl, W.H. *In situ* high-resolution photoelectrochemical imaging of precursor sites for pitting in polycrystalline titanium. *J. Electrochem. Soc.,* **1999**, *146*(7), 2495-2501.
http://dx.doi.org/10.1149/1.1391961

[199] Dai, N.; Zhang, L.-C.; Zhang, J.; Chen, Q.; Wu, M. Corrosion behavior of selective laser melted Ti-6Al-4V alloy in NaCl solution. *Corros. Sci.,* **2016**, *102*, 484-489.
http://dx.doi.org/10.1016/j.corsci.2015.10.041